Proximity-dependent labeling identifies dendritic cells that prime the antitumor CD4$^+$ T cell response

Aleksey Chudnovskiy[1], Sandra Nakandakari-Higa[1], Tiago BR Castro[1], Ang Cui[2], Chia-Hao Lin[3], Moshe Sade-Feldman[2], Brooke K. Phillips[1], Juhee Pae[1], Luka Mesin[1], Juliana Bortolatto[1], Lawrence D. Schweitzer[2], Giulia Pasqual[4], Li-Fan Lu[3], Nir Hacohen[2,5], Gabriel D. Victora[1,*]

[1] Laboratory of Lymphocyte Dynamics, The Rockefeller University, New York, NY, USA.

[2] Broad Institute of MIT and Harvard, Cambridge, MA, USA.

[3] Division of Biological Sciences, University of California, San Diego, La Jolla, CA, USA.

[4] Laboratory of Synthetic Immunology, Oncology and Immunology Section, Department of Surgery Oncology and Gastroenterology, University of Padua, Padua, Italy.

[5]Center for Cancer Research, Massachusetts General Hospital, Boston, MA, USA.

* Address correspondence to victora@rockefeller.edu.

Abstract

Dendritic cells (DCs) are uniquely capable of transporting tumoral antigens to tumor-draining lymph nodes (tdLNs), where they initiate antitumor immunity and mediate checkpoint blockade immunotherapy. Despite recent advances, the full phenotype of the DCs involved in these processes has been difficult to establish. Using LIPSTIC (Labeling Immune Partnerships by SorTagging Intercellular Contacts)-based single-cell transcriptomics, we identify individual DCs capable of presenting antigen to CD4$^+$ T cells in the tdLN. These represent a small fraction of all DCs present in the tdLN and display a distinctive activated phenotype that includes production of cytokine IL-27, required for efficient T cell priming and tumor rejection. Tumor progression results in loss of effective priming of naïve CD4$^+$ T cells, downstream of transcriptional changes in DCs that are manifested already when they arrive at the tdLN. Collectively, our data reveal temporal shift in DC activation status over the course of the antitumor immune response.

Introduction

When properly activated, T cells can exert powerful control over cancer, as evidenced by decades of work that culminated in checkpoint-blockade immunotherapies[1–3]. As with other adaptive immune processes, the quality of the T cell response towards a tumor is heavily dependent on the identity and phenotype of the DCs that present tumor-derived antigens to T cells in the tumor draining lymph node (tdLN). DCs are divided into migratory DCs, capable of transporting antigens acquired in the tumor to the tdLN, and resident DCs, which have access only to antigen that arrives to LN through lymphatics or that is handed over to them by their migratory counterparts[4–7]. Both populations can be further subdivided along an orthogonal axis into conventional (c)DC1 and cDC2 subsets, based on their phenotype and ontogeny[5,8]. Generally speaking, cDC1s have higher capacity to prime $CD8^+$ T cells, whereas migratory cDC2s are best at priming $CD4^+$ T cells[9–11], although these distinctions are far from absolute[12].

Both cDC1s and cDC2s have been implicated as drivers of the antitumor immune response[9,13]. Mice lacking cDC1s show enhanced tumor growth concomitant with reduced tumor-specific effector $CD8^+$ T cells[11,14–17]. $CD4^+$ T cell priming by cDC2s is suppressed by regulatory T (Treg) cells[18], and Treg depletion unleashes a cDC2-driven $CD4^+$ T cell response to the tumor[13]. Moreover, checkpoint inhibitors do not work efficiently in the absence of DCs, highlighting the role of antigen presentation as a major driver of the response to immunotherapy[11,15,19]. More recent studies have identified a novel DC state termed "mature DCs enriched in immunoregulatory molecules" (mRegDCs)[20]. DCs in this state have enhanced capacity to take up antigens but reduced ability to prime antitumor T cell responses. mRegDC share many common genes with the novel "cDC3" subset described in humans[21,22], and further work is needed to clearly delineate the cDC3 and mRegDC states[23].

Despite the central role they play in determining the quality of the antitumoral response, technical challenges in measuring cell–cell interactions *in vivo* have prevented a fine characterization of the individual DCs responsible T cell priming in this context[4], limiting our understanding to the coarser level of whole DC populations. Resolution beyond the population level would be especially important for our understanding of cDC2 programs, given the greater

heterogeneity of phenotypes and lineages among this subset[24,25]. To address such questions, we previously developed LIPSTIC (Labeling Immune Partnerships by SorTagging Intercellular Contacts), a proximity-based labeling method based on transfer between interacting cells of a labeled substrate detectable by flow-cytometry that allows us to identify and isolate DCs engaged in T cell priming *in vivo*[26]. By combining LIPSTIC with single-cell RNA sequencing (scRNA-seq), we performed interaction-based transcriptomic profiling of the DCs responsible for priming tumor-specific $CD4^+$ T cells. Our data show that a minor population of DCs, characterized by a hyperactivated transcriptional program, accounted for most T cell priming in the tdLN. DCs with this phenotype were lost over time as tumors grew, which correlated with loss of effective T cell priming. Together, our data point towards the progressive suppression of DC activation as an additional strategy for tumor immune evasion.

Results

LIPSTIC identifies DCs capable of priming naïve $CD4^+$ T cells in response to tumor antigens

LIPSTIC relies on the *S. aureus* transpeptidase sortase A (SrtA) to transfer an injectable biotinylated peptide substrate (biotin-LPETG) between pairs of cells interacting via the CD40L-CD40 pathway. SrtA, fused to the extracellular domain of CD40L expressed on $CD4^+$ T cells, captures substrate injected *in vivo* and transfers it onto five N-terminal glycines engineered into the extracellular domain of CD40 (G_5-CD40) on interacting DCs (**Fig. 1A**). To apply this system to a solid tumor model, we engineered the B16 melanoma cell line[27] to express the $OVA_{323-339}$ (OT-II) peptide ($B16^{OT-II}$; **Fig. S1A**). We then inoculated G_5-CD40-expressing mice (*Cd40*$^{G5/G5}$) subcutaneously with 10^6 $B16^{OT-II}$ cells in the flank region to generate a response in the tumor-draining inguinal lymph node (tdLN). At 9 d.p.i., we adoptively transferred 3 x 10^5 CD40L-SrtA OT-II T cells into tumor-bearing mice, carrying out LIPSTIC labeling of the tdLN by local injection of biotinylated LPETG substrate at 10-12 h after T cell transfer (**Fig. 1B**), a point at which T cell interaction with DCs is exclusively cognate[26]. This system allows transferred OT-II T cells to serve as "reporters" that specifically identify and label the subset of DCs capable of priming naïve $CD4^+$ T cells at that time point.

This approach revealed that a minor population (approximately 5 to 10%) of DCs acquired the LIPSTIC label in the tdLN of mice bearing B16^{OT-II} tumors but not in controls inoculated with the parental B16 line (B16 WT) (**Fig. 1C**). In agreement with previous findings[10,26], LIPSTIC labeling in the tdLN was detected exclusively on migratory (CD11c^{Int}MHC-II^{Hi}) but not resident (CD11c^{hi}MHC-II^{int}) DCs (**Fig. 1D and S1B**). The specificity of LIPSTIC labeling was confirmed by injection of a blocking antibody to CD40L (clone MR1) 2 h prior to substrate injection, which fully abrogated labeling (**Fig. 1E**). Mixed bone marrow chimera experiments in which a fraction of DCs were deficient for MHC-II confirmed that LIPSTIC captures predominantly interactions driven by antigen presentation in this setting (**Fig. S1C**). Thus, LIPSTIC labeling in the B16 system is antigen-specific and dependent on the CD40L–CD40 interaction. DCs of both XCR1^{+}CD11b^{-} (cDC1) and XCR1^{-}CD11b^{+} (cDC2) phenotypes (**Fig. 1F**) were labeled by OT-II T cells, at a ratio that corresponded roughly to the total cDC2/cDC1 ratio in each tdLN. This suggests that both subsets of DCs are equally capable of priming tumor antigen-specific CD4^{+} T cells, a notion supported by previous findings in the literature[12,13]. Because our B16^{OT-II} cell line also expresses GFP (**Fig. S1A**), we were able to simultaneously probe DCs for interaction with CD4^{+} T cells and for the extent to which they carry intact tumor-derived proteins. Although there was a statistically significant enrichment in biotin^{+} cells among the GFP^{+} DC population, GFP and LIPSTIC labeling were overall poorly correlated (**Fig. 1G**). Thus, the storage of intact tumor-derived antigen does not fully overlap with the ability to use this antigen to prime naïve CD4^{+} T cells in vivo, possibly due to the specific kinetics of antigen storage and presentation over time.

To ascertain that LIPSTIC^{+} DCs indeed carried the antigen necessary to prime antigen-specific T cells, we set up a miniaturized assay in which 150 tdLN-derived biotin^{+} DCs were co-cultured *ex vivo* with 750 CFSE-labeled OT-II CD4^{+} T cells in the absence of exogenous antigen. This approach showed that biotin^{+} DCs were exclusively capable of driving T cell proliferation above the background levels obtained with DCs derived from mice carrying parental B16 melanomas that lacked the OT-II peptide (**Fig. 1H**). An analogous experiment with OVA-specific CD8^{+} (OT-I) T cells (using a B16 line that we engineered to express a transmembrane version of the full OVA protein, B16^{mOVA}) showed that, again, biotin^{+} tdLN DCs were exclusively capable of driving T cell proliferation (**Fig. 1H**). We conclude that LIPSTIC labeling faithfully identifies the

DCs capable of presenting antigen to both CD4⁺ and CD8⁺ T cells within the tdLN, and that such DCs represent only a minor fraction of all DCs available at that site.

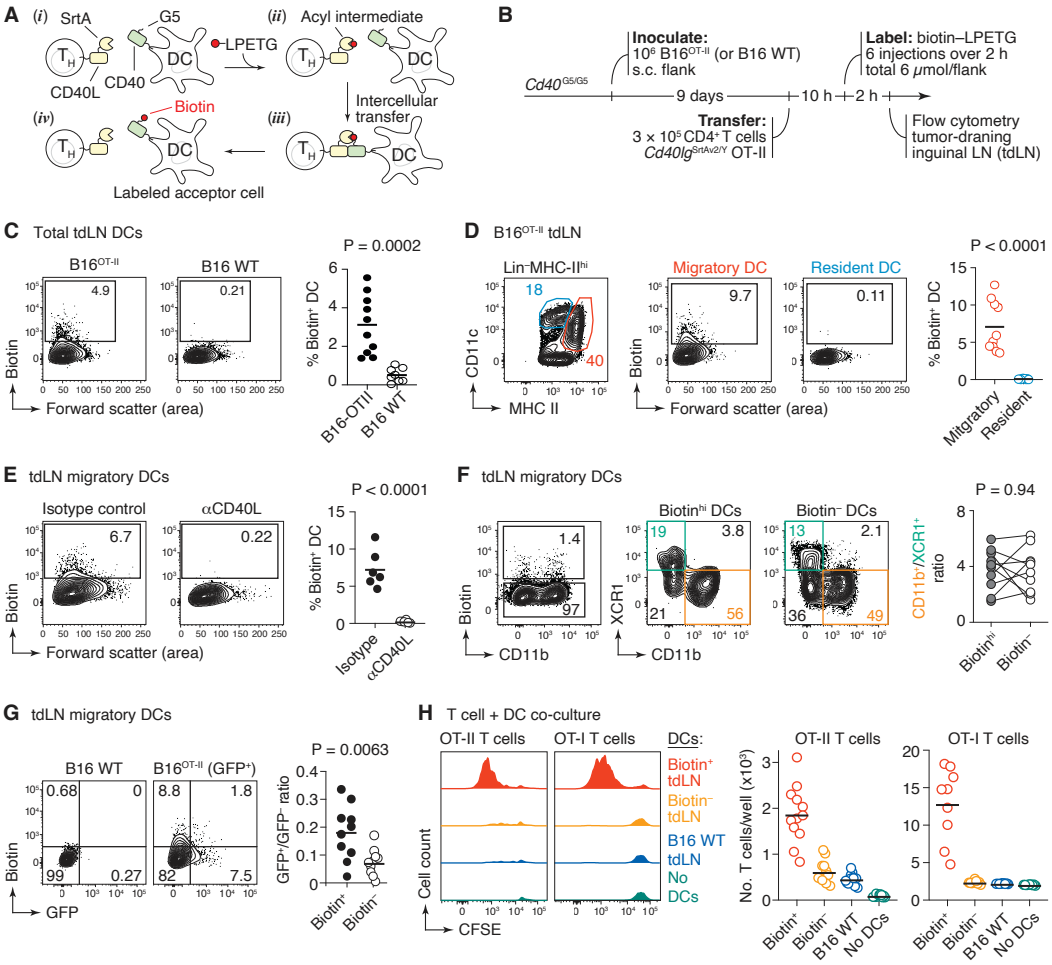

Figure 1. Using LIPSTIC to identify tumor antigen-presenting DCs. (A) Schematic of the LIPSTIC system. T cells expressing *S. aureus* transpeptidase sortase A (SrtA) fused to CD40L transfer an injectable biotinylated peptide substrate (biotin-LPETG) onto five N-terminal glycines engineered into the extracellular domain of CD40 (G_5-CD40) on interacting DCs. **(B)** Experimental setup for panels (C-G). In (C, D, F, G) bilateral tumors were injected) **(C)** Percentage of labeled DCs in mice bearing $B16^{OTII}$ or parental B16 tumors (left) and quantification of data (right) (n = 5, 4 mice per group). **(D)** Gating on resident and migratory DCs in tdLN (left), percentage of labeled migratory and resident DCs in tdLN (center), and quantification of data (n = 5 mice) (right). **(E)** Percentage of labeled DCs in mice treated with isotype control antibody vs. anti-CD40L antibody (left) and quantification of data for (n = 6 mice per group) (right). **(F)** Contour plots (left, center) showing percentage of cDC1 and cDC2 among biotin⁺ and biotin⁻ DCs and quantification of data for (right) (n = 5 mice). **(G)** Percentage of GFP⁺ and biotin⁺ DCs in tdLN (left) and quantification of GFP⁺ DCs among biotin⁺ and biotin⁻ DCs in tdLN (n = 5 mice). (C, D, F, G each symbol represents one LN), E each symbol represents one mouse. **(H)** Proliferation of OT-II and OT-I T cells in vitro after 96 h of co-culture with DCs derived from mice carrying $B16^{OT-II}$ or $B16^{OVA}$ tumors, respectively (left) and quantification of T cells per well at the end of the culture period (right). For (H) tdLN were pooled from (n = 6-10 mice) each dot represents one culture well. P-values are for unpaired t test, except (F), where paired t test was used.

DCs capable of priming naïve CD4⁺ T cells are in a distinct activated state

To understand what distinguishes DCs capable of CD4⁺ T cell priming in tdLNs beyond a population-level analysis, we transcriptionally profiled individual biotin⁺ and biotin⁻ migratory DCs obtained from tdLNs at 9 and 15 d.p.i. and control DCs from steady-state iLNs by plate-based single cell mRNA sequencing (scRNA-seq). DCs fell into five transcriptional clusters (**Fig. 2A; Spreadsheet S1**), of which two expressed signatures associated with a cDC1 phenotype (Clusters 1 and 3) and three to a cDC2 phenotype (Clusters 0, 2, and 4) (**Fig. S2A**). Few differences were noted when comparing biotin⁻ migratory DCs sorted from B16$^{OT\text{-}II}$ tdLNs or total migratory DCs from steady-state iLNs. On the other hand, biotin⁺ tdLN DCs, especially those with a cDC2 phenotype, were strongly enriched in Cluster 0, which consisted almost exclusively of LIPSTIC-labeled cells (**Fig. 2B and C**). Similar but less pronounced segregation of biotin⁺ and biotin⁻ phenotypes was observed within cDC1 Cluster 3 **(Fig. 2B)**. In both cDC1 and cDC2 populations, LIPSTIC labeling correlated with expression of CD40 target genes[28], as expected from DCs capable of priming a CD4⁺ T cell response and given the pathway assayed by the LIPSTIC method (**Fig. S2B**).

Differential gene expression comparing biotin⁺ and biotin⁻ tdLN DCs showed significant modulation of 269 genes (224 upregulated and 45 downregulated). Of these, 136 were commonly modulated in biotin⁺ cDC1 and cDC2 populations and 66 changed exclusively in biotin⁺ cDC2 (**Fig. S2C** and **Spreadsheet S2**). Changes included upregulation of genes encoding for classic markers of DC maturation (*Cd80*, *Cd86*, *Cd40*, *Cd82*) and of nuclear factor (NF)-κB activation (*Nfkbiz*, *Tnfaip3* (A20))[29,30], typical of an activated DC state (**Fig. 2D**). Genes functionally important for T cell priming were also upregulated, including *Cd1d1*, cytokines *Tnf* and *Ebi3*, drivers of DC–T cell interaction such as *Sema4a* and *Alcam*[31–34], and the proteasome activator involved in antigen presentation (*Psme2b*)[35]. *Ifitm3*, *Tmem39a*, and *Tmem173* (STING), genes important for infectious disease and autoimmunity[36–38]. Notably, LIPSTIC-labeled DCs, especially cDC2s, upregulated several genes related to cell migration and microanatomical localization of DCs and T cells, including the chemokines *Ccl17*, *Ccl22*, *Ccl9*, and *Ccl6*[39–43], *Gpr183* (encoding the G-protein-coupled receptor EBI2, a critical guidance receptor that positions DCs at the LN follicle border and splenic bridging channels[44–46]), and cell motility regulators such as *Msn* (moesin) and

Cd81 (**Fig. 2D**). On the other hand, biotin$^+$ DCs downregulated several genes expressed in anti-inflammatory DCs and/or associated with the induction of T cell tolerance, such as *Tbc1d4*, *Mfge8*, and *Cblb*[24,47,48] (**Fig. 2D**). We confirmed findings pertaining to individual genes at the level of entire gene signatures obtained from the "Gene Ontology" and "Hallmark" MSigDB databases[49,50]. Biotin$^+$ cDC1s and especially cDC2s showed higher expression of inflammation/activation signatures as well as of signatures related to cell migration, motility, and regulation of the actin cytoskeleton (**Fig. 2E and Spreadsheet S3**). Finally, although biotin$^+$ DCs expressed higher levels of the "mRegDC" and "cDC3"[20,51] signatures, overlap between our Biotin$^+$ LIPSTIC signature and these two gene sets was only moderate, indicating that both programs are related but not identical to that of LIPSTIC-labeled DCs (**Fig. S2D ,E**).

To determine whether DCs with a similar activated phenotype could be detected in tdLNs in the absence of exogenous T cell transfer, we generated a "LIPSTIC$^+$" signature consisting of the 224 genes most highly upregulated in biotin$^+$ compared to biotin$^-$ DCs (**Spreadsheet S4**). We then applied this signature to a previously published set of single-cell transcriptomes of tdLN myeloid cells obtained at 14 days post-inoculation with B16 melanoma, either in control conditions or after depletion of Treg cells using a *Foxp3*^{DTR} mouse allele. The LIPSTIC signature was expressed predominantly by one group of cells in this dataset (Cluster 6), corresponding to cDC2-phenotype DCs (**Fig. 2F**). Notably, although DCs from control tdLN were also present, the large majority of cells in this group (87.5%) originated from Treg-depleted mice (**Fig. 2G**). Conversely, comparison of DCs from control and Treg-depleted settings showed upregulation of the LIPSTIC signature in cDC2s and to a lesser extent cDC1s, while DCs in Cluster 6 expressed this signature equally regardless of whether they originated in control or Treg-depleted mice (**Fig. 2H**). We conclude that DCs with a LIPSTIC-like phenotype can be detected in low numbers in the tdLNs of tumor-bearing mice in the absence of T cell transfer and increase in abundance upon depletion of Treg cells.

Together, our data indicate that DCs actively engaged in the priming of CD4$^+$ T cells represent a transcriptionally unique population with activated DC features and increased expression of locomotion and migration genes, suggestive of enhanced ability to colocalize with T

cells in LN regions conducive to T cell priming. Our analysis further suggests that acquisition of this activated phenotype by DCs is actively suppressed by the presence of Treg cells.

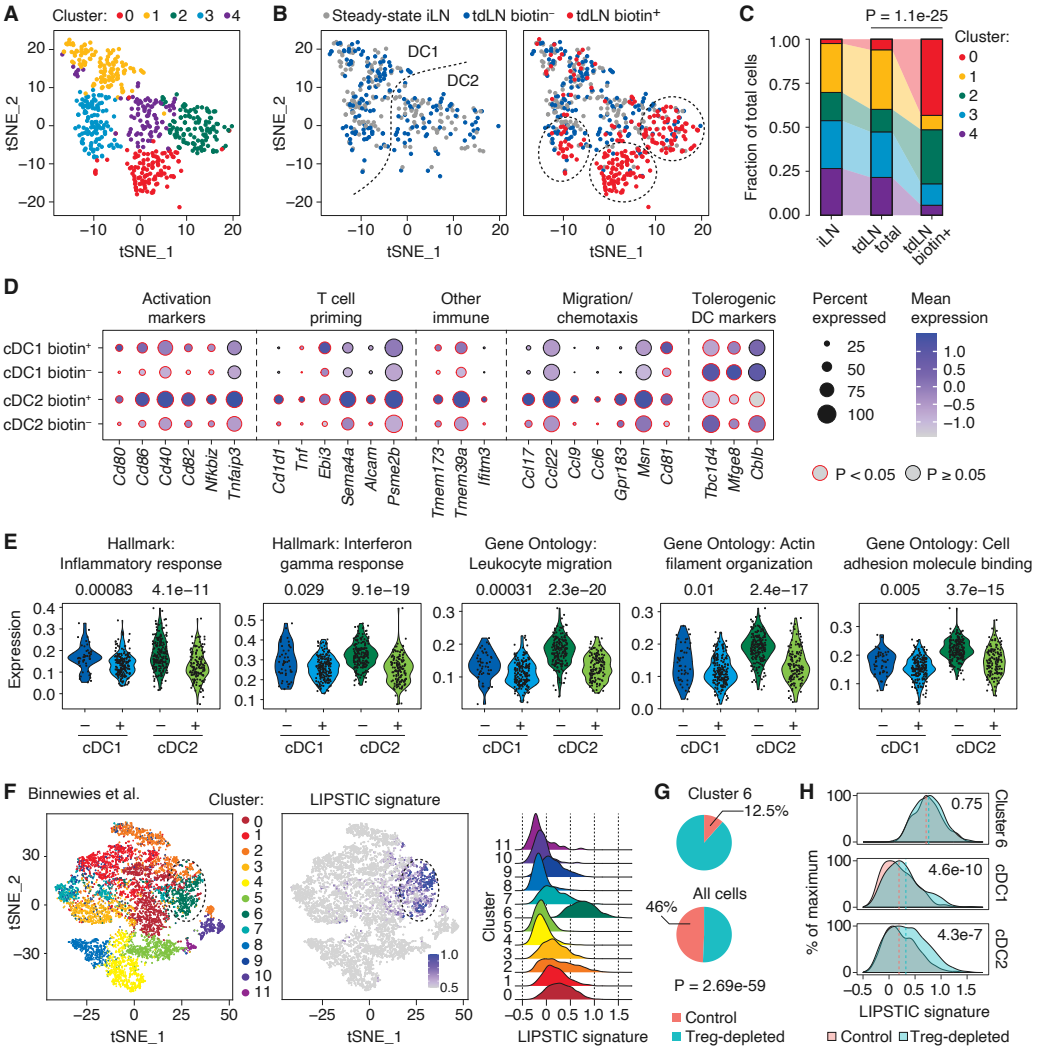

Figure 2. Biotin⁺ DCs represent a transcriptionally distinct DCs state. (A) t-distributed stochastic neighbor embedding (t-SNE) scatter plot showing clustering of DCs sorted from tdLN or steady-state iLN. Cells are pooled from 2 steady-state and 2 tumor-bearing mice from 2 independent experiments. **(B)** Distribution of steady-state iLN, biotin⁻ tdLN and biotin⁺ tdLN DCs in the same plot. Dotted lines indicate the approximate location of the cDC1/cDC2 boundary (left) and of Cluster 0 (right). **(C)** Proportion of cells in each transcriptional cluster among steady-state, biotin⁻ and biotin⁺ DCs. **(D)** Expression of genes significantly upregulated in both biotin⁺ cDC1 and cDC2 compared to biotin⁻ cDC1 and cDC2. **(E)** Violin plots showing most upregulated gene signatures in both biotin⁺ cDC1 and cDC2 compared to biotin⁻ cDC1 and cDC2. **(F)** t-SNE scatter plot showing clustering (left) and expression of a LIPSTIC⁺ gene signature (center) among tdLN myeloid cells under control conditions or upon depletion of Treg cells. Right, expression of the LIPSTIC+ signature by cluster. **(G)** Percentage of DCs from control vs. Treg-depleted conditions in Cluster 6 vs. in all cells. **(H)** Expression of the LIPSTIC⁺ signature in DCs from control or Treg depleted mice in Cluster 6 among total cDC1 and cDC2. Data in (F-H) are from Binnewies et al.[13]. Pearson's chi-squared test was used for (C and G) Wilcoxon signed-rank test was used for (D, E and H). All experiments in this figure used the *Cd40lg*^{SrtAv1} allele.

IL-27 produced by priming-competent DCs promotes an effective antitumoral response

Among the most highly upregulated genes in Cluster 0 at 9 d.p.i. were *Ebi3* and *Il27*, which encode for EBI3 and p28—the two subunits of the cytokine IL-27 (**Figs. 3A and S2C**). IL-27 is a pleiotropic cytokine that can take on pro- or anti-inflammatory roles depending on the setting[52,53], and has been shown to either promote or suppress tumor growth in different experimental models[54,55]. To investigate the effects of IL-27 in our setting, we treated mice 9 days after subcutaneous inoculation of $B16^{OT\text{-}II}$ cells with either a blocking antibody to p28 or an isotype control. One day later, we adoptively transferred OT-II T cells into tumor bearing mice and followed the fate of these cells as they were primed within the tdLN and infiltrated the tumor (**Fig. 3B**). In the tdLN, blocking p28 reduced the ability of OT-II T cells to produce CXCR3 and IFNγ, critical mediators of Th1 effector function[56] (**Fig.3C**). In agreement with the role of CXCR3 in promoting effector T cell trafficking to the tumor site[17,57], p28 blockade reduced OT-II T cell recruitment to the tumor, coinciding with a decrease in production of IFNγ by this population (**Fig. 3D**). Parallel experiments using $B16^{OVA}$ showed that anti-p28 treatment also reduced IFNγ production by OT-I $CD8^+$ T cells in both tdLN and tumor, although no difference in expression of CXCR3 or tumor infiltration was observed (**Fig. S3B,C**). To assess the significance to the anti-tumoral response of the loss of T cell effector function upon p28 blockade, we used our engineered $B16^{mOVA}$, which showed delayed growth kinetics in comparison with $B16^{OT\text{-}II}$ and was often completely rejected by the host (**Fig. S1A**). Treatment of mice inoculated with $B16^{mOVA}$ with p28 blocking antibody starting at 2 d.p.i. (**Fig. 3E**) resulted in increased tumor size and weight when compared to control-treated mice (**Fig. 3F**). To determine whether IL-27 produced by DCs was required for this antitumor immunity, we inoculated $B16^{mOVA}$ cells into CD11c (Itgax)-cre *Il27*$^{flox/flox}$ mice, in which DCs are deficient in production of IL-27. Although baseline rejection of $B16^{mOVA}$ tumors was less pronounced in control *Il27*$^{flox/flox}$ mice lacking cre recombinase (possibly due to differences in the mouse housing environment at UCSD, where these experiments were performed), tumor growth was still significantly increased in mice lacking DC production of IL-27 (**Fig. 3G**) compared to controls. We conclude that IL-27 produced by DCs is required for full priming of $CD4^+$ T cells and for antitumor immunity in this setting.

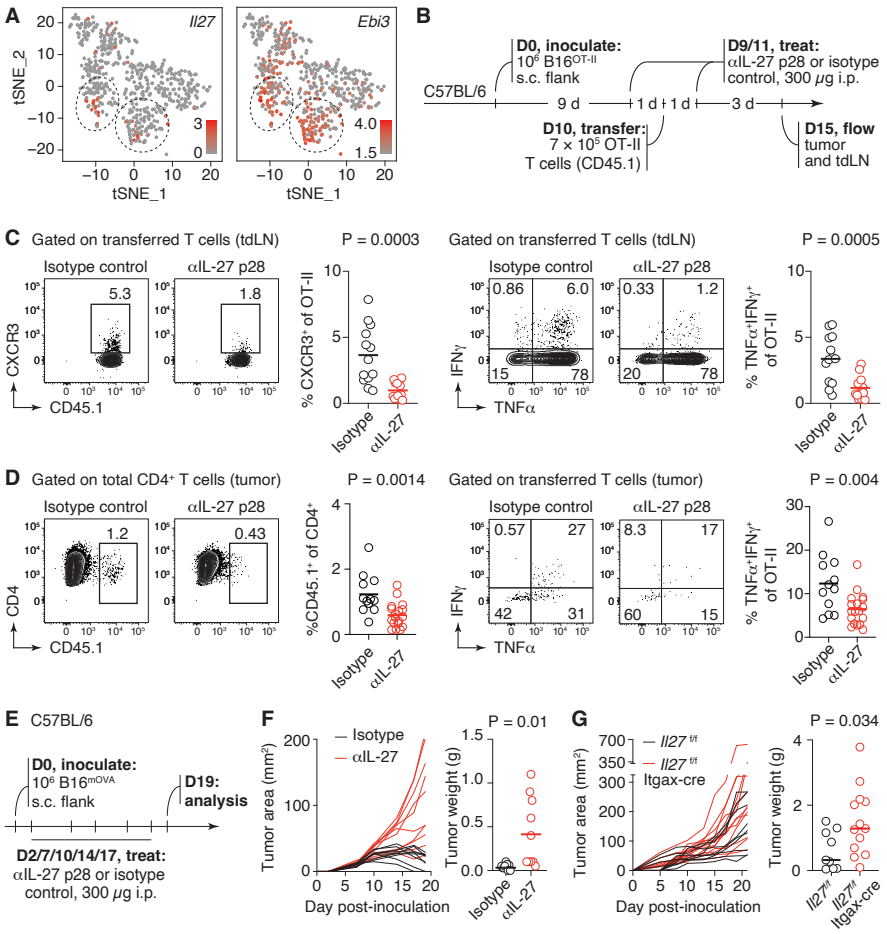

Figure 3. *Il27* promotes an antitumor CD4⁺ T cell response and drives antitumor immunity. (A) Expression of *Il27* and *Ebi3* in DCs. t-SNE plot as in Fig. 2A. **(B)** Schematic for IL-27 (p28) blocking in mice bearing B16$^{OT\text{-}II}$ tumors. **(C)** Expression of CXCR3⁺ (left) or TNFα and IFNγ (right) among OT-II T cells in tdLN of isotype or anti-p28-treated mice. Graphs summarize data from 2 independent experiments with (n= 13 mice per group.) **(D)** Percentage of OT-II cells among all CD4⁺ T cells (left) and expression of TNFα and IFNγ among OT-II T cells (right) in the tumors of isotype or anti-p28-treated mice. Graphs summarize data from 2 independent experiments with (n = 12 and 18 mice per group). **(E)** Schematic for IL-27 (p28) blocking in mice bearing B16^{mOVA} tumors. (**F**) Tumor growth curves and tumor weights for isotype control and anti-p28-treated groups (n = 9, 10 mice per group). **(G)** Tumor growth curves and tumor weights for *Il27*$^{f/f}$ (control) and *Il27*$^{f/f}$ Itgax-Cre groups. Data are from 4 independent experiments with n = 9 (control) and n=13 (*Il27*$^{f/f}$ Itgax-Cre). P-values are for unpaired t test

DC priming and activation status is rapidly lost with tumor progression

During their development, tumors progressively suppress multiple arms of the immune response to establish a state of tolerance to tumor antigens[18,58–62]. To verify if the ability of DCs to prime CD4⁺ T cells was also subject to such suppression, we performed LIPSTIC labeling of tdLN at early (day 9) and late (day 15) time points after tumor inoculation, following the model described in Figure 1B. In line with tumor-mediated suppression, LIPSTIC labeling of migratory DCs

decreased by 50% between 9 and 15 d.p.i. (**Fig. 4A and B**). This decrease was of equal magnitude in cDC1s and cDC2s (**Fig. 4A and B**). To extend this observation to a second tumor model, we engineered the MC-38 colon adenocarcinoma cell line[63] to express the OT-II peptide (MC-38^{OT-II}; **Fig. S1A**). As with B16 tumors, LIPSTIC labeling of MC-38^{OT-II} by OT-II T cells also decreased with time, again with comparable reductions in cDC1 and cDC2 populations (**Fig. 4C and D**). Thus, DCs lose capacity to prime naïve CD4$^+$ T cells over a short period of time in two different implantable tumor models.

In addition to the reduction in the proportion of LIPSTIC$^+$ DCs with time, analysis of our scRNA-seq data—which contained tdLN DCs obtained at both day 9 and day 15 post-tumor inoculation—showed that DCs from different time points occupied different positions in transcriptional space (**Fig. 4E**). Specifically, there was a pronounced reduction in DCs expressing the activated "Cluster 0" program (**Fig. 2A**) at the later time point (**Fig. 4E and F**). Thus, DCs capable of priming CD4$^+$ T cells at late time points were not only less abundant, but also less activated than their early counterparts. To determine whether loss of Cluster 0 DCs at late time points had functional consequences for T cell priming, we adoptively transferred naïve CD4$^+$ OT-II T cells into B16^{OT-II}-bearing recipient mice at 9 or 14 d.p.i.. Five days after cell transfer, we observed a greater extent of upregulation of classical exhaustion markers PD-1, Lag3, and TIGIT on T cells transferred at the late compared to the early time point (**Fig. 4G**). Transcriptional profiling of bulk OT-II T cells primed early and late after tumor injection showed that T cells primed at the early time point were enriched in pathways associated with inflammatory responses and cytokine activity (*Cxcl10*, *Cd83*, *Rel, Nfkbid*, *Il2*, *Lta*) and expressed higher levels of genes directly suppressed by Foxp3 (such as *Il2* and *Tnfsf11*)[64], although *Foxp3* itself was not detected in any sample in this dataset. By contrast, T cells primed at the late time point showed higher expression of cell cycle-associated genes, possibly reflecting increased abundance of antigen (**Fig. 4H and S4 and Spreadsheet S5**). We conclude that tumor progression is associated with loss of antigen presentation to CD4$^+$ T cells, primarily by highly-activated "Cluster 0" DCs, and that this loss coincides with an impairment in the priming of activated CD4$^+$ T cells.

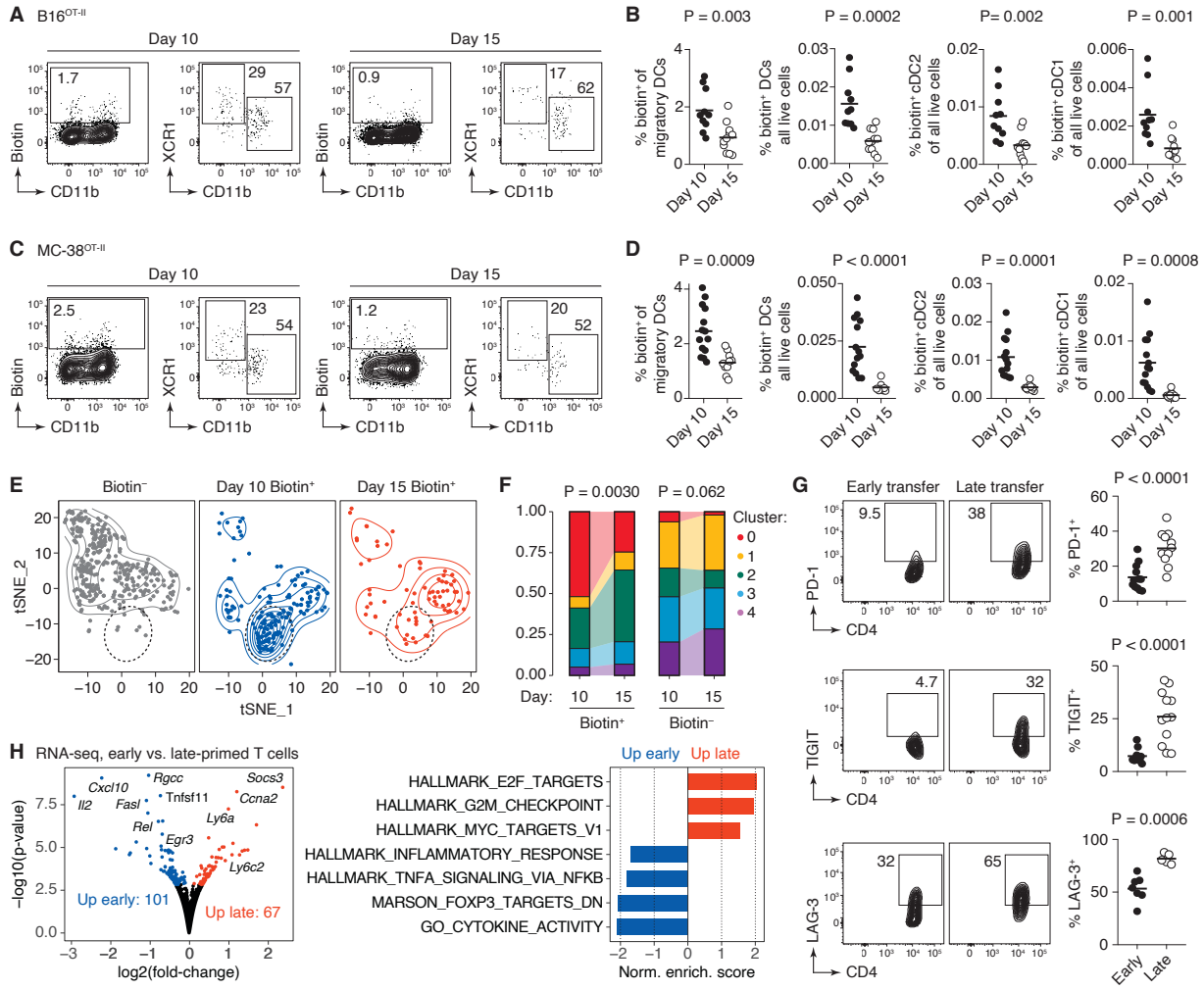

Figure 4. DCs lose priming capacity as tumors progress. (A) Percentage of biotin⁺ DC and cDC1/cDC2 distribution in tdLN of mice bearing B16$^{OT\text{-}II}$ tumors at 10 (early) or 15 (late) d.p.i. **(B)** Quantification of data as in (A) (n = 10 mice per group from 4 independent experiments, each dot represent one mouse). Experiments in (A-D) used the *Cd40lg*^{SrtAv1} allele. **(C-D)** as in (A-B) but in mice bearing MC-38$^{OT\text{-}II}$ tumors (n= 7 mice per group, with bilateral tumors; each dot represents one tdLN). **(E)** t-SNE contour density plots showing distribution of biotin⁻ (left) and biotin⁺ DCs at 10 (center) or 15 (right) d.p.i. in tdLN of B16$^{OT\text{-}II}$ bearing mice. Dotted circles indicate the approximate location of Cluster 0 (Fig. 2A). **(F)** Distribution of transcriptional clusters from Fig. 2A among biotin⁺ and biotin⁻ DCs from 10 and 15 d.p.i. Data for (E-F) are from the experiment described in Fig. 2A. **(G-H)** Tumor-specific OT-II T cells were transferred into mice bearing B16$^{OT\text{-}II}$ tumors at 10 or 15 d.p.i. and assayed 5 days later by flow cytometry for **(G)** (n= 12 mice per group from 2 independent experiments for PD-1 and TIGIT, n = 7 and 5 mice per group for LAG-3)) or scRNA-seq (7 mice from one experiment). (G) Expression of exhaustion markers PD-1, TIGIT, and LAG-3 OT-II T cells transferred at 10 or 15 d.p.i. (H) Differentially expressed genes (left) or gene signatures (right) between OT-II T cells transferred at 10 or 15 d.p.i. P-values are for Pearson's chi-squared test (F) or unpaired t test for B, D and G.

Late loss of DC priming capacity occurs prior to DC arrival at the tdLN

To determine whether loss of DC activity resulted from a generally immunosuppressive environment within the tdLN (e.g., due to accumulation of tumor-derived soluble mediators or regulatory cells[65], or from a defect intrinsic to the individual DCs arriving from the tumor, we first assessed the ability of the tdLN to support a $CD4^+$ T cell response unrelated to the tumor. We inoculated *Cd40*$^{G5/G5}$ mice with parental B16 melanoma cells (lacking the OT-II peptide) and adoptively transferred *Cd40lg*$^{SrtA/Y}$ OT-II T cells into these mice at 14 d.p.i. One day later, we immunized recipient mice with OVA in alum adjuvant in the base of the tail, a site that targets both the tdLN and the contralateral non-draining LN (**Fig. 5A,B**). We found no significant difference in the ability of tdLN DCs to prime $CD4^+$ T cells (as read out by LIPSTIC labeling) compared to DCs in the contralateral LN (**Fig. 5C**). Thus, the loss of DC ability to prime $CD4^+$ T cells at late time points in tumor development is not driven by broad immunosuppression within the tdLN environment.

An alternative explanation for the loss of DC priming capacity with time is that suppression is intrinsic to the DCs arriving at the tdLN from the tumor. To verify this, we used an in-situ photoconversion protocol similar to one previously described in the literature[66] to directly measure the state of DCs arriving from the tumor to the tdLN at early and late time points. We injected mice ubiquitously expressing the photoconvertible *Kikume* green-to-red (KikGR) protein[67,68] with MC-38^{OT-II} cells, which allow efficient photoactivation due to the lack of the dark pigmentation characteristic of B16 tumors (**Fig. 5D**). Photoactivation of tumors under a 415 nm LED source at 9 and 14 d.p.i. led to accumulation of photoconverted migratory, but not resident, DCs in the tdLN as early as 16 h post-photoconversion (**Fig. 5E and S5A**), allowing us to isolate DCs immediately after they arrived at the tdLN from the tumor. We performed scRNA-seq profiling of photoconverted DCs sorted from tdLN at 10 and 15 d.p.i. (i.e., 16 h after photoactivation at 9 and 14 d.p.i. respectively; **Fig. 5F-H**). DCs from both early and late time points were broadly distributed across three major transcriptional clusters, with noticeable enrichment of day 10 DCs in Cluster 2, composed primarily of cDC2-phenotype cells (**Fig. 5F and S5B**). There was a measurable reduction in the expression of both the $LIPSTIC^+$ and the original "Cluster 0" signatures (see **Fig. 2 and Spreadsheet S4**) in DCs obtained from the late time point (**Fig. 5G**).

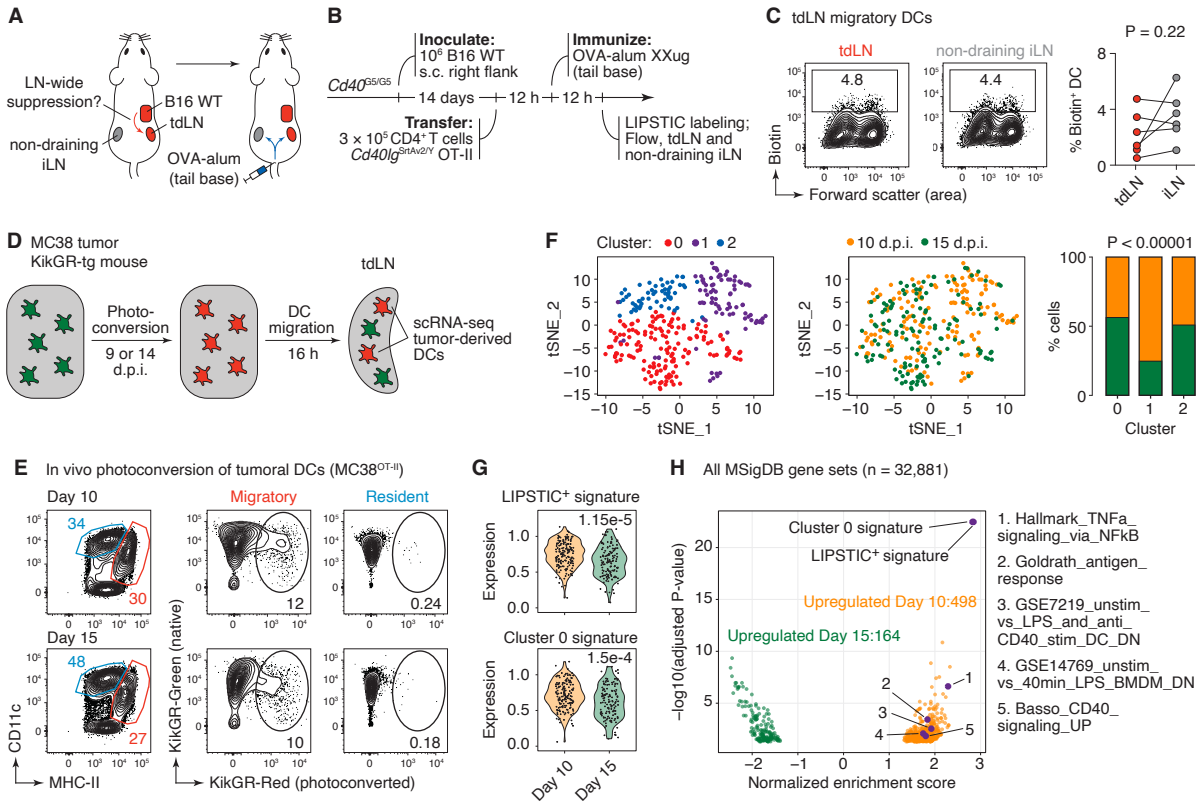

Figure 5. Late tumor-derived DCs are dysfunctional upon arrival at the tdLN. (A) Cartoon and **(B)** schematic of the immunization experiment in (C). **(C)** Percentage of biotin⁺ DCs in tdLN and non-draining iLN (left) and quantification of data (n=6 mice) (right). **(D)** Cartoon depicting tumor photoconversion (PC) experiment. **(E)** Percentage of PC migratory and resident DCs in tdLN at 10 (early, top) and 15 (late, bottom) d.p.i with (n = 6 mice per group) representative plots are shown. **(F)** t-SNE scatter plot showing clustering of photoactivated DCs according to whole transcriptome analysis (left) and distribution of early and late DCs (center). (Right) distribution of early and late DCs within each cluster. **(G)** Expression of the LIPSTIC⁺ and Cluster 0 gene signatures (Fig. 2; Spreadsheet S4) in early vs late DCs. **(H)** Expression in early and late DCs of LIPSTIC⁺ and Cluster 0 gene signatures in the context of all gene sets in the MSigDB database. Numbers in the plot refer to the signatures listed on the right. Data for (G-H) are for (n =6 mice per group) profiled in a single sequencing experiment.(C) P values were calculated using paired t-test, (F) Pearson's chi-squared test, (G) Wilcoxon signed-rank test.

Querying this dataset for differential expression of the entire 32,881 gene signature collection available in the MSigDB database (v.7.5.1)[49,50] showed that both the LIPSTIC⁺ and the Cluster 0 gene signatures were better able to discern early and late photoconverted DCs than any other set in the database, including several signatures related to CD40 or NF-κB activation (**Fig. 5H and Spreadsheet S6**). Thus, a major distinction between DCs arriving in the tdLN from the tumor at early and late time points is the expression of genes in the LIPSTIC⁺ signature, indicative of their ability to prime a CD4⁺ T cell response. We conclude that the loss of CD4⁺ T cell priming capacity that arises at later stages of tumor development is not due to a generally

immunosuppressive tdLN environment, but rather results from a qualitative shift in the activation status of the DCs that likely takes place before they migrate to the tdLN from the tumor site.

We conclude that tumor progression correlates with a loss of the ability of DCs to engage strong activation programs and present antigen to naïve $CD4^+$ T cells, likely due to changes in the state of migratory DCs prior to their arrival at the tdLN.

Discussion

A challenge in studying the priming capabilities of DCs has been the heterogeneity in their phenotypes, even within canonical DC populations[24,69]. Whereas the literature is plentiful in associations between the broader populations of DCs (such as cDC1 and cDC2, or migratory and resident DCs) and the priming of specific types of T cell responses[12,70,71], studies that characterize the individual DCs directly engaged in T cell priming are rare[72]. LIPSTIC provides an easy and highly quantitative method to identify and profile engaged DCs at the individual cell level. As such, LIPSTIC provides degree of specificity to DC research analogous to that afforded to B and T cell studies by antigen tetramers[73,74].

Our LIPSTIC data revealed that the fraction of all tdLN DCs that actively engage in priming $CD4^+$ T cell responses to a subcutaneously implanted tumor is quite small, on the order of 5-10% of the DCs in the LN even at the early time point peak. These DCs are almost entirely of the migratory DC phenotype and are not enriched in cDC1 or cDC2 when compared to the entire LN DC population. In co-culture experiments, $biotin^+$ DCs were exclusively able to prime both $CD4^+$ and $CD8^+$ T cells. This indicates that the DCs that prime $CD8^+$ T cells responses *in vivo* are included within the DC population labeled by $CD4^+$ T cells, suggesting substantial overlap between these populations. Thus, CD40L LIPSTIC is unlikely to be missing any DC populations capable of priming exclusively $CD8^+$ T cells. Our findings contribute to a series of active discussions in the field regarding the numbers and population-level phenotypes of the DCs that prime the antitumoral T cell response[6,12,13,20,757].

A potential limitation of LIPSTIC is that it identifies only DCs that engage T cells through the CD40L-CD40 pathway. Most if not all conventional $CD4^+$ T cells are thought to express CD40L even in their naïve state[76] and to upregulate its expression upon antigen-driven activation[77]. Conversely, most DCs express CD40, although its expression by resident DCs is generally lower than by DCs with migratory phenotype[78]. Nevertheless, because the CD40L-CD40 axis is critical for DC activation and licensing for cross-presentation[79–82], CD40L LIPSTIC is likely to identify most or all DCs that are potent presenters of immunogenic tumor antigens. This notion is supported by our miniaturized DC culture assays, in which LIPSTIC-negative DCs were unable able to induce proliferation of $CD4^+$ or $CD8^+$ T cells above background levels, indicating that most antigen available to be presented *in vivo* is concentrated within the $LIPTSIC^+$ DC population.

Interaction-based transcriptional profiling of LIPSTIC-labeled cells showed that priming-capable DCs expressed a unique transcriptional profile that separated them from other DCs in the tdLN. Notably, total DCs from tdLN were indistinguishable transcriptionally from DCs obtained from a naïve iLN, implying that this population of DCs, or at least their prominent role in T cell priming, would not be identifiable without LIPSTIC. The ability to prime T cells was associated with upregulation of multiple genes important for DC activation and antigen presentation. These included classic DC maturation markers such as *Cd80*, *Cd86*, and *Cd40* itself[83], indicative of partial overlap with the canonical "mature DC" phenotype[84]. However, LIPSTIC-labeled DCs also upregulated multiple genes and signatures associated with cell migration, adhesion, and T cell chemotaxis[85]. Thus, the ability of DCs to access specific microanatomical compartments and to recruit T cells to these areas, previously shown to be functionally important for T cell responses[44–46,86], is in fact one of the defining characteristics of the DCs capable of engaging T cells *in vivo*. Intersecting our transcriptional data with a much larger scRNA-seq data set of tdLN myeloid cells[13], revealed a cluster of DCs with strong expression of the $LIPSTIC^+$ signature. A small fraction of this cluster represented DCs found in the tdLN under control non-manipulated conditions—indicating that the $LIPSTIC^+$ transcriptional state is not a product of our specific setup (e.g., of the adoptive transfer of a relatively large number of tumor antigen-specific T cells). More importantly, however, the large majority of cells in this cluster consisted of DCs that appeared upon ablation of Treg cells using a DTR transgene. These findings suggest that one of the effects of Treg cells,

possibly potentiated in the tumor microenvironment, is to prevent DCs from acquiring a LIPSTIC$^+$-like state. Of note, the cytokine IL-27 was among the most upregulated gene products in LIPSTIC$^+$ DCs. IL-27 is an especially pleiotropic cytokine, which has been shown to prime both tolerogenic and immunogenic T cell responses under different conditions[52–55,87–91]. In our settings, IL-27 produced by DCs was essential for priming IFNγ production by tumor-specific CD4$^+$ and CD8$^+$ T cells, recruitment of effector T cells to the tumor site, and control of tumor growth. This result agrees with previous reports in the literature and disagrees with others under similar settings[54,55]. The reasons for these discrepancies remain unclear and merit further investigation.

We observed a pronounced decrease in LIPSTIC labeling of DCs over a short period of time from 10 to 15 days post-tumor inoculation, which correlated with an almost complete loss of DCs with the activated "Cluster 0" signature. Tumor growth was thus associated with an abrupt loss of DC activation and priming capacity, even as the load of tumor-derived antigen increased. The local environment of the tdLN itself appears not to be responsible for loss of DC fitness, since immunization of tumor-draining and non-draining LN with a non-tumoral antigen led to equal LIPSTIC labeling at both sites. On the other hand, *in vivo* photoconversion experiments showed that DCs arriving from the tumor to the tdLN at late time points strongly downregulated gene signatures associated with LIPSTIC labeling, to the extent that changes in expression of LIPSTIC-related gene signatures appear to be the primary distinction between DCs that arrive at the tdLN at early vs. late time points. Together, these observations indicate that the state in which DCs arrive at the tdLN over time changes, implicating the tumor microenvironment—possibly including innate maturation stimuli[92] or signals delivered by help from tumor-infiltrating effector CD4$^+$ T cells and/or suppressed by Treg cells—in setting the maturation state and priming capability of tdLN DCs.

In conclusion, LIPSTIC allowed us, for the first time, to identify the individual DCs capable of priming CD4$^+$ T cells in the course of tumor development and to define transcriptional programs associated with this capability and how they change over time. The *in vivo* DC activation signature identified in this work has the potential to be exploited practically to improve responses to tumoral antigens by therapeutic targeting of DCs or their products. In addition, we expect that

the LIPSTIC interaction-based transcriptomics platform laid out in this study will be useful for immunologists wishing to identify the DCs that prime $CD4^+$ T cell responses in various settings.

Acknowledgments

We thank A. Kamphorst (Mount Sinai School of Medicine) and C. Brown (Memorial Sloan Kettering Cancer Center) for critical reading of our manuscript; Z. Yin (Nankai University) for *Il27*^{flox} mice; C. Brown for the B16^{OVA} cell line; K. Gordon for cell sorting; the Rockefeller University Genomics Center for RNA sequencing and Comparative Biosciences Center for animal housing; and Rockefeller University employees for their continuous assistance. This work was supported by NIH grant DP1AI144248 and the Hirschl/Weil-Caulier Research Award (G.D.V.), Starr Consortium grant I10-044 (N.H. and G.D.V.) and NIH grants AI108651 and AI163813 (L.-F.L.). Work in the Victora Laboratory is supported by the Robertson Foundation. A.C. was supported by a Damon Runyon Postdoctoral Fellowship. G.D.V. is a Pew-Stewart Scholar, a Burroughs-Wellcome Investigator in the Pathogenesis of Infectious Disease, and a MacArthur Fellow.

Author contributions

A.C. designed and performed most experiments, with assistance from G.P., B.K.P., J.P., and L.M.. S.N.-H. and J.B. generated *Cd40lg*^{SrtAv2} mice. T.B.R.C. and A.C. performed all computational analyses. M. S.-F. and L.D.S. generated single-cell RNA-seq libraries under supervision of N.H. C.-H.L. and L-F.L. designed and performed experiments on *Il27*-deficient mice. N. H. and G.D.V. designed and supervised experiments. G.D.V. and A.C. wrote the manuscript with input from all authors.

Conflict of Interest

L.-F.L. is a scientific advisor for Elixiron Immunotherapeutics. G.D.V. has a U.S. patent on LIPSTIC technology (US10053683). G.D.V. is a scientific advisor for Vaccine Company, Inc.

Methods

Mice

Cd40^{G5} mice were generated as described[26] and maintained in our laboratory. Two versions of *Cd40lg*^{SrtA} mice were used, the original conditional version[26] (which we refer to as *Cd40lg*^{SrtAv1}) and a new constitutive *Cd40lg*^{SrtAv2} version (see below). Unless indicated in the figure legend, all experiments are done using the constitutive version. C57BL6/J, CD45.1 (B6.SJL Ptprca), *H2*$^{-/-}$ [93], CD4-Cre-transgenic[94], and OT-I TCR transgenic[95] mice were purchased from The Jackson Laboratory (strains 000664, 002014, 003584, 022071, and 0003831, respectively). OT-II TCR-transgenic mice (Y chromosome version)[96] mice were bred and maintained in our laboratory. *Il27*^{flox} [91] and Itgax-cre[97] mice were bred and maintained at UCSD. CAG-KikGR-transgenic mice[67] were a gift from A. Hadjantonakis (Memorial Sloan Kettering Cancer Center). CAG-KikGR-transgenic mice were back-crossed to the C57BL6 background for at least 10 generations at Rockefeller University. All mice were housed in specific pathogen-free conditions, in accordance with institutional guidelines and ethical regulations. All protocols were approved by the Rockefeller University or UCSD Institutional Animal Care and Use Committees. Male and female mice aged 5–12-weeks were used in all experiments.

Generation of Cd40lg^{SrtAv2} *mice*

Cd40lg^{SrtAv2} mice were generated in our laboratory using the EASI-CRISPR method[98]. Cas9-crRNA-tracrRNA complexes targeting the last exon of the *Cd40lg* locus (GAGTTGGCTTCTCATCTTT) were microinjected along with a single-stranded DNA templates encoding a C-terminal SrtA fusion flanked by 200bp homology arms into the pronuclei of fertilized C57BL6 embryos, which were then implanted into pseudopregnant foster dams. Founder mice were backcrossed to WT C57BL6 mice for at least 5 generations to reduce the probability of transmitting CRISPR-induced off-target mutations.

Generation of transgenic tumor lines

Constructs were cloned into the pMP71 vector[99], which was modified to express a fluorescent reporter (eGFP) followed by sequence encoding amino acids 323-339 of chicken OVA (eGFP-OT-II) or the *thosea asigna* virus self-cleaving 2A peptide (T2A)[100] followed by the full-length OVA protein (eGFP-OVA). Retroviruses were produced in HEK-293 cells using $CaCl_2$ transfection. Gag-Pol and VSV plasmids were used for virus packaging. Virus-containing supernatant was harvested 48 h after transfection, spun down at 252 XG for 5 min, and filtered through a 0.45 µm filter. B16-OT-II or B16-OVA™ melanoma cell lines or MC38-OT-II colon adenocarcinoma were produced by retroviral transduction with eGFP-OT-II or eGFP-OVA™ constructs. Briefly, viral supernatant from HEK-293 cells was added to B16 or MC-38 cells with 5 mg/ml of polybrene (Sigma-Aldrich H9268) and cells were spun down at 800 XG for 90 minutes at 30 degrees. Viral supernatant was replaced with regular medium 12 h after transfection. 60 h after transfection, eGFP^{+} cells were sorted using a FACSAria II, expanded, and frozen in liquid nitrogen.

Murine tumor models.

All tumor cell lines were grown in DMEM supplemented with 1% L-Glutamine and 1% Penicillin/Streptomycin. On the day of tumor injection, tumor cells were trypsinized with TrypLE express, washed twice, and resuspended in sterile PBS. Mice were anesthetized and shaved on one or both

flanks, and one million of tumor cells were injected in 50 µl of PBS subcutaneously (unilaterally or bilaterally) at a site adjacent to the inguinal lymph. Tumor growth was assessed 2-3 times per week by caliper measurements. Tumor area was calculated by multiplying tumor length and tumor width.

Adoptive cell transfers

To isolate $CD4^+$ or $CD8^+$ T cells, spleens were forced through 70 µm filters, red blood cells were lysed with ACK buffer (Lonza), and $CD4^+$ or $CD8^+$ T cells were isolated using $CD4^+$ or $CD8^+$ T cells isolation kits (Miltenyi Biotec) as described in the manufacture protocols. Purified cells were injected intravenously in 100 µl of PBS.

LIPSTIC in vivo.

Biotin-aminohexanoic acid-LPETGS, C-term amide, 95% purity (biotin-LPTEG) was purchased from LifeTein (custom synthesis) and stock solutions prepared in PBS at 20 mM. For LIPSTIC labeling in vivo, biotin–LPETG was injected subcutaneously into the flank (shaved area proximal to tumor and iLN). 50 µl of 20 mM substrate dissolved in PBS (equivalent to 1 µM/injection) were injected a total of six times (6 µM total) 20 min apart, and iLN were collected 20 min after the last injection, as described previously[26]. Mice were briefly anaesthetized with isoflurane before each injection.

Antibody treatment.

For IL-27 blocking experiments, animals were injected intraperitoneally with 300 µg of p28 blocking antibody clone (BioXcell MM27.7B1) or isotype control clone (BioXcell C1.18.4). The regimen for each experiment is described in the corresponding figure legend. For CD40L-blockade experiments, mice were injected intravenously with 200 µg of CD40L-blocking antibody (clone MR-1, BioXCell) two hours prior to the first injection of substrate.

Immunization

For immunization experiments, mice were immunized by subcutaneous injection into the base of the tail with 25 µg OVA adsorbed in alum (Imject Alum, Thermo Fisher Scientific) at 2:1 antigen:alum (v:v) ratio in 50 µl volume.

Surgery and KikGR photoconversion

Tumor-bearing animals were anaesthetized with isoflurane, shaved, and washed with ethanol and 0.005M iodine solution. The tumor was completely exposed by an incision made on the side distal to the iLN. Photoactivation was performed by exposing the tumor to 415 nM light for three minutes using a custom-built Prizmatix LED source. The incision was then closed using FST autoclips.

Bone marrow chimeras

WT C57BL6/J mice were lethally irradiated with two doses of 450 rad from an X-ray source, administered five hours apart. Animals were reconstituted by intravenous injection of hematopoietic cells obtained from bone-marrows of donor mice. Chimeric mice were used in experiments 7-12 weeks after irradiation.

Flow cytometry and cell sorting.
iLN were collected and cut into small pieces in microfuge tubes. For digestion, iLN were incubated for 30 min at 37 °C in HBSS (Gibco) supplemented with $CaCl_2$, $MgCl_2$, and collagenase D (Roche). After digestion, tissue was forced 5 times through a 21 Gauge needle (BD) and filtered through a 70 µm strainer into a 15 ml falcon tube. Tumors were excised, cut into small pieces and digested with collagenase D and DNase I for 1 h at 37 °C in HBSS (Gibco). After digestion, tumors were forced 10 times through a 21 gauge needle (BD) and filtered through a 70 µm strainer into a 50 ml falcon tube. Tumors were spun down and resuspended in 3 ml 10% Percoll/RPMI, which was layered on top of 90% Percoll/RPMI. Cells were spun down for 25 min at 615 XG at 20°C with breaks off. The gradient interface containing leukocytes was collected and washed with 15 ml of PBE buffer. Single-cell suspensions were washed with PBE and incubated at room temperature for 5 min with 1 µg/ml anti-CD16/32 (2.4G2, BioXCell). Cells were stained for surface markers on ice in 96-well plates for 15 min in PBE, using the reagents listed in Table S1. Cells were washed with PBE and stained with Zombie fixable viability dyes (Biolegend) at room temperature for 15 min, then fixed with Cytofix (BD Biosciences). For biotin–LPETG SrtA substrate staining, an anti-biotin–PE antibody (Miltenyi Biotec) was exclusively used as described [26]. Samples were acquired on Symphony, Fortessa or LSR-II flow cytometers or sorted on FACSAriaII or FACSAriaIII cell sorters (BD Biosciences). Data were analyzed using FlowJo v.10.6.2 software.

In vitro DC-T cell co-culture
Mice were injected with the indicated tumors. On day 10, animals were injected with substrate as described above, and biotin$^+$, biotin$^-$, or total migDCs from OVA$^-$ tumors (150 DCs for OT-II and 500 DCs for OT-I cultures) were sorted into U-bottom 96-well plates. 750 CD4$^+$ OT-II and 2500 CD8$^+$ OT-I CFSE-labeled splenic T cells were sorted in the corresponding wells. All wells contained RPMI supplemented with 1% Penicillin/Streptomycin, 1% Sodium Pyruvate, 1% non-essential amino acids, 1% HEPES. For OT-II cell cultures, RPMI media was supplemented with 2% T-stim media with ConA (Avantor). All cells were transferred into FACS tubes and the entire sample was recorded to determine cell numbers.

Library preparation for scRNA-seq and bulk RNA sequencing.
Libraries were prepared using the Smart-Seq2 method, as previously described[101]. In brief, RNA from single-sorted cells was extracted using RNAClean XP Solid Phase Reversible Immobilization (SPRI) beads (Beckman Coulter). Extracted RNA was first hybridized using an RT primer (/5BiosG/AAGCAGTGGTATCAA
CGCAGAGTACTTTTTTTTTTTTTTTTTTTTTTTTTTTTTTVN), then reverse transcribed into cDNA using a TSO primer (59-AAGCAGTGGTATCAACGCAGAGTACATrGrGrG-39) and RT maxima reverse transcriptase (Thermo Fisher Scientific). Amplification of cDNA was performed using an ISPCR primer (59-AAGCAGTGGTATCAACGCAGAGT39) and KAPA HiFi HotStart ReadyMix (Thermo Fisher Scientific). Amplified cDNA was cleaned up three times using RNAClean XP SPRI beads. cDNA was tagmented using the Nextera XT DNA Library Preparation Kit (Illumina). For each sequencing run, up to four plates were barcoded at a time with Nextera XT Index Kit v2 Sets A–D (Illumina). Dual-barcoded libraries were pooled and sequenced using Illumina Nextseq 550 platform. Bulk RNA sequencing was performed as for scRNA-seq except that 700 cells were sorted per well.

Transcriptomic analysis

scRNA-Seq libraries were processed using RSEM for sequencing read quantification and STAR for the transcriptome alignment. For our single-cell studies, quantification matrices were loaded into the R environment and processed using the Seurat package pipelines[102]. Briefly, cells containing more than 10% of their reads mapped to mitochondrial DNA were filtered out. In addition, we also removed single-cell contaminants that expressed known markers of B-cells, T-cells, and macrophages. In total, 562 cells were selected for downstream analysis for our LIPSTIC experiment and 299 cells for our photoactivation experiment. For both experiments, cells were log normalized, and the top 2,000 variable genes were selected for data scaling and PCA construction. During data scaling, the library size and the mitochondrial percent were regressed-out to remove unwanted variation sources. After PCA construction, the JackStraw algorithm available in Seurat was used to select the most significant principal components. Finally, cells were clustered and visualized in t-SNE space. For signature analysis, the AddModuleScore function was used to determine the average expression of a gene list compared to a background control. Gene set enrichment analysis (GSEA) was performed in the R environment using the fgsea package [103] to determine pathway enrichment. Signature sets obtained from MSigDB were used as input with a pre-ranked list based on log2 fold change. Signatures were considered enriched if the adjusted p-value had a value of at least 0.05. To determine commonly activated genes in LIPSTIC positive cDC1 and cDC2 cells, we used a LIPSTIC signature as a pathway and the pre-ranked comparison between cDC1 (positive x negative) and cDC2 (positive x negative). We then compared the two LIPSTIC positive leading edges for matching and exclusive genes. For external data analysis, data was downloaded from the GEO database, accession code: GSE125680[13]. To apply our LIPSTIC signature, we used the AddModuleScore function available with the Seurat package. We used the top 20 genes enriched in biotin positive DCs compared to biotin negative DCs, or the top 20 genes enriched in Cluster 0, compared to the remainder of the cells.

Bulk RNA-Seq data was aligned and quantified using STAR. The count matrix was used within the R environment and processed using the DESeq2 package[104]. Genes from samples expressing less than 10 reads were pre-filtered. Gene expression among samples was normalized by applying a negative binomial distribution model. Differential gene expression was determined by the Wald test, genes with adjusted FDR <0.1 were considered for downstream analysis, and log2 fold changes were shrunk using the ashr algorithm[105]. Finally, GSEA was performed in the pre-ranked mode using the fgsea package as previously described.

Statistical analysis

All statistical analyses was performed using data from at least three biological replicates, with the exact number of replicates stated in each figure legend. Unless stated otherwise, all statistical analyses were performed using Graphpad Prism v.8 software. Unpaired Student's t test was used for most pairwise comparisons, except instances indicated in figure legends where paired Student t test or Wilcoxon signed-rank test were used. For experiments involving more than two groups of animals one-way ANOVA was used with Tukey's test comparing the means of every treatment to the means of every other treatment. Differences with p-values < 0.05 were considered as statistically significant.

Table S1. Antibodies used for flow cytometry

Antibody	Clone	Cat. #	Vendor
BUV 395 anti-mouse CD279	J43	744549	BD
BUV 395 anti-mouse CD45	30-F11	564279	BD
BUV 395 anti-mouse CD45.1	A20	565212	BD
BUV 395 anti-mouse CD45.1	A20	565212	BD
BUV 395 anti-mouse I-A/I-E	2G9	743876	BD
BV 421 anti-mouse CD279 (PD-1)	29F.1A12	135221	BioLegend
BV 421 anti-mouse CD4	GK1.5	100438	BioLegend
BV 421 anti-mouse CD64	X54-5/7.1	139309	BioLegend
BV 421 anti-mouse I-A/I-E	M5/114.15.2	107632	BioLegend
BV 421 Rat Anti-Mouse CD40	3/23'	562846	BD
BV 605 anti-mouse CD45.2	104	109841	BioLegend
BV 605 anti-mouse CD86	GL-1	105037	BioLegend
BV 605 anti-mouse CD8α	53-6.7	100744	BioLegend
BV 711 anti-mouse CD3ε	145-2 C11	100349	BioLegend
BV 711 anti-mouse CD4	RM4-5	100557	BioLegend
BV 711 anti-mouse/human CD11b	M1/70	101242	BioLegend
BV 785 anti-mouse CD3	17A2	100232	BioLegend
BV 785 anti-mouse NK-1.1	PK136	108749	BioLegend
BV 785 anti-mouse/human CD45R/B220	RA3-6B2	103246	BioLegend
PE anti-biotin	Bio3-18E7	130-113-291	Miltenyi
PE anti-mouse CD183 (CXCR3)	CXCR3-173	126505	BioLegend
PE anti-mouse TNFα	MP6-XT22	506306	BioLegend
PE/Cy7 anti-mouse CD223 (LAG-3)	C9B7W	125226	BioLegend
PE/Cy7 anti-mouse CD45.1	A20	110730	BioLegend
PerCP-eFluor 710 TIGIT	GIGD7	46-9501-80	Invitrogen
PerCP/Cy5.5 anti-mouse CD80	16-10A1	104722	BioLegend
PerCP/Cy5.5 anti-mouse/rat XCR1	ZET	148208	BioLegend
APC anti-mouse CD11c	N418	117310	BioLegend
APC anti-mouse CD64	X54-5/7.1	17-0641-82	eBioscience
APC anti-mouse IFNγ	XMG1.2	17-7311-82	Invitrogen

Supplementary Figures

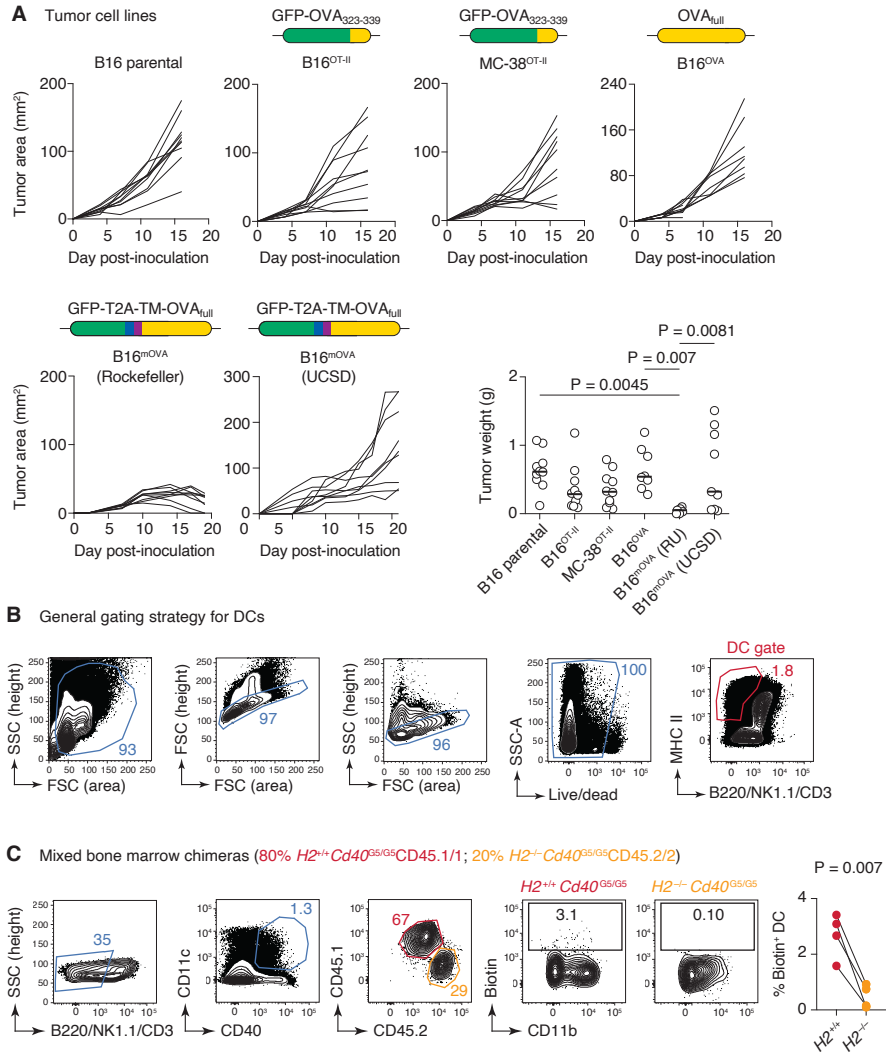

Figure S1. Experimental setup and additional controls. (A) B16 melanoma and MC-38 colon adenocarcinoma cell lines were transduced with the indicated constructs and injected into recipient mice. Tumor growth curves are shown for each indicated tumor line, compared to the previously generated parental B16 and B16^{OVA} lines. The B16mOVA line was grown in mice housed either at the Rockefeller University or at UCSD for different experiments (See Fig. 3, from which the growth and weight data are reproduced). Graph at bottom right shows tumor weight for each indicated tumor line. P-values were calculated using one-way ANOVA followed by Tukey's multiple comparison test for the means; only p-values < 0.05 are shown. **(B)** Contour plots showing the general gating strategy for tdLN DCs prior to gating on MHC-II/CD11c. **(C)** Mixed chimeras were generated with 80% *H2*$^{+/+}$.*Cd40*$^{G5/G5}$ and 20% *H2*$^{-/-}$.*Cd40*$^{G5/G5}$ bone marrow cells transferred into lethally-irradiated WT C57BL6 mice. Contour plots show the gating strategy for MHC-II-deficient DCs and percentage of biotin^{+} DCs in tdLN in each donor population. Right, quantification of biotin^{+} DCs among MHC-II-sufficient and -deficient DCs in (n = 4 mice). P-value is for paired T-test.

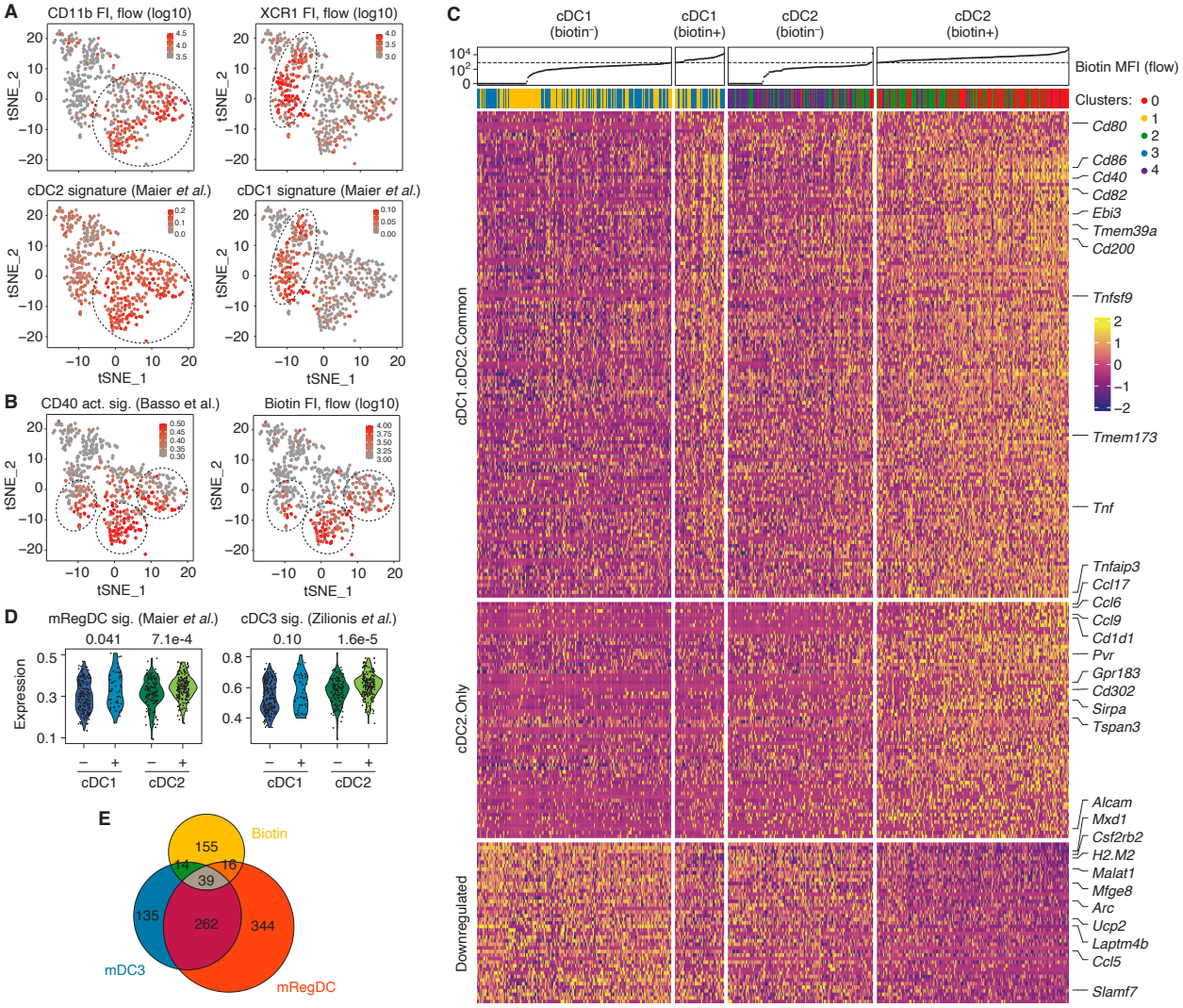

Figure S2. Single-cell transcriptomics of tdLN DCs. (A) Fluorescence intensity (FI) of CD11b and XCR1 staining (top) and expression of cDC1 and cDC2 gene expression signatures among DCs. t-SNE plot as in Fig. 2A. FI data were obtained from flow cytometry index-sorting files; cDC1 and cDC2 signatures were obtained from the literature[20]. **(B)** As in (A), showing a signature of CD40 activation in B cells[28](left) and biotin FI (LIPSTIC signal) from index sorting (right). **(C)** Heatmap showing expression of genes significantly modulated in biotin⁺ vs. biotin⁻ DCs. The uppermost rows show biotin FI from flow cytometry, followed by transcriptional clusters as shown in Fig. 2A. Genes are sorted into 3 clusters corresponding to genes upregulated in biotin⁺ cDC1 and cDC2 (top), genes upregulated in biotin⁺ cDC2 only (middle) and genes downregulated in biotin⁺ cDC1 and cDC2 (bottom). Selected genes are indicated in the right. **(D,E) (D)** Expression of mRegDC and cDC3 signatures from the literature[20,51] among biotin⁺ and biotin⁻ cDC1 and cDC2. **(E)** Venn diagram of the overlap between LIPSTIC⁺, cDC3, and mRegDC signatures. Wilcoxon signed-rank test was used to measure P value for (D-E).

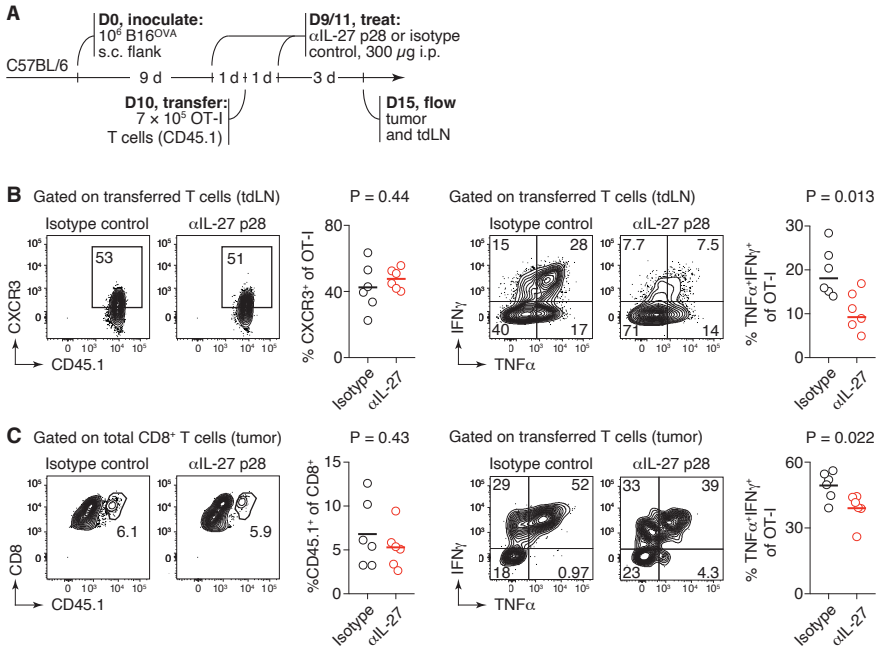

Figure S3. IL-27 blockade enhances CD8⁺ T cell priming. (A) Schematic for IL-27 (p28) blocking in mice bearing B16^{OVA} tumors. **(B)** Contour plots and quantification showing percentages of CXCR3 positive cells among transferred OT-I cells in tdLN (left). (Right) contour plots and quantification showing percentages of IFNγ^+ TNFα^+ among OT-I cells in tdLN. Graphs summarize data for (n = 6 mice per group). **(C)** Percentage of OT-I cells among all CD8$^+$ T cells (left) and expression of TNFα and IFNγ among OT-I T cells (right) in the tumors of isotype or anti-p28-treated mice. Graphs summarize data for (n = 6 mice per group)

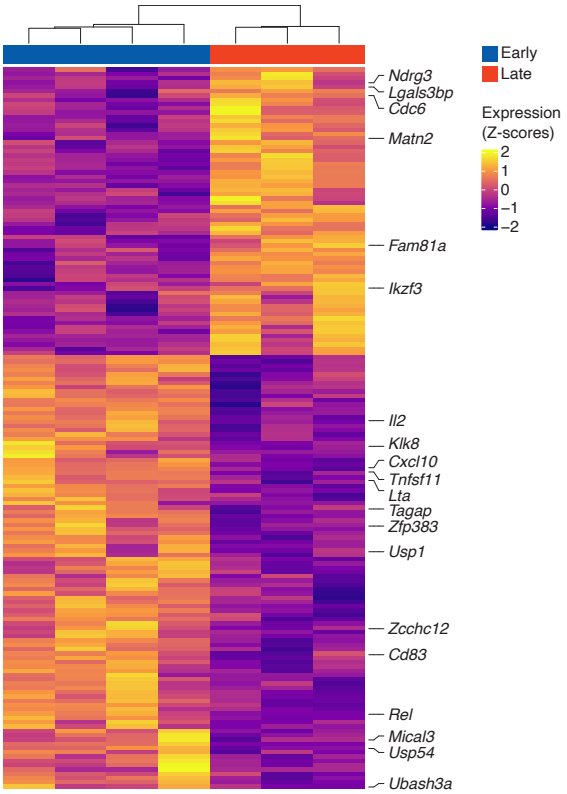

Figure S4. Gene expression changes in early- vs. late-primed CD4⁺ T cells. Heatmap showing expression of genes significantly modulated in OT-II T cells primed at 10 or 15 days after inoculation of mice with B16$^{OT\text{-}II}$ tumors. Selected genes are indicated in the right.

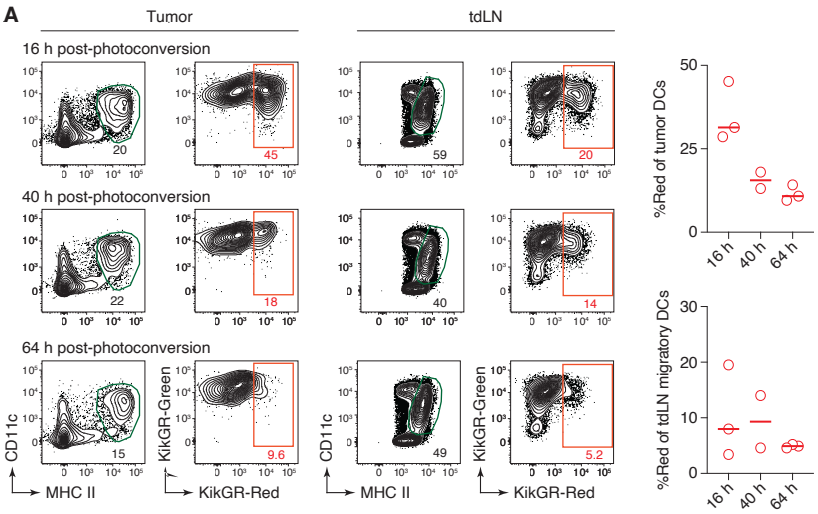

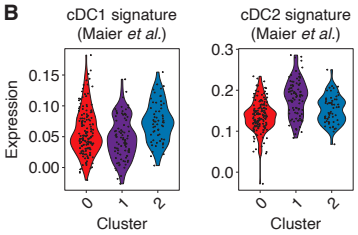

Figure S5. *In vivo* photoconversion of tumor resident DCs. (A) Contour plots showing percentage of photoconverted DCs at the indicated time points after photo conversion in tumor or tdLN (left). (Right) quantification of percentage of photoconverted DCs in the tumor or in the tdLN. (n = 2-3 mice per time point). (**B**) Violin plots showing cDC1 or cDC2 signatures (Maier et al.) in each cluster (refer to Fig 5).

References

1. Leach, D. R., Krummel, M. F. & Allison, J. P. Enhancement of antitumor immunity by CTLA-4 blockade. *Science (80-.).* (1996). doi:10.1126/science.271.5256.1734
2. Sharma, P. & Allison, J. P. Immune checkpoint targeting in cancer therapy: Toward combination strategies with curative potential. *Cell* **161**, 205–214 (2015).
3. DeVita, V. T. & Rosenberg, S. A. Two Hundred Years of Cancer Research. *N. Engl. J. Med.* (2012). doi:10.1056/nejmra1204479
4. Chudnovskiy, A., Pasqual, G. & Victora, G. D. Studying interactions between dendritic cells and T cells in vivo. *Current Opinion in Immunology* (2019). doi:10.1016/j.coi.2019.02.002
5. Merad, M., Sathe, P., Helft, J., Miller, J. & Mortha, A. The Dendritic Cell Lineage: Ontogeny and Function of Dendritic Cells and Their Subsets in the Steady State and the Inflamed Setting. *Annu. Rev. Immunol.* (2013). doi:10.1146/annurev-immunol-020711-074950
6. Wculek, S. K. *et al.* Dendritic cells in cancer immunology and immunotherapy. *Nature Reviews Immunology* (2020). doi:10.1038/s41577-019-0210-z
7. Ruhland, M. K. *et al.* Visualizing Synaptic Transfer of Tumor Antigens among Dendritic Cells. *Cancer Cell* (2020). doi:10.1016/j.ccell.2020.05.002
8. Murphy, T. L. *et al.* Transcriptional Control of Dendritic Cell Development. *Annu. Rev. Immunol.* (2016). doi:10.1146/annurev-immunol-032713-120204
9. Hildner, K. *et al.* Batf3 deficiency reveals a critical role for CD8α+ dendritic cells in cytotoxic T cell immunity. *Science (80-.).* (2008). doi:10.1126/science.1164206
10. Roberts, E. W. *et al.* Critical Role for CD103+/CD141+ Dendritic Cells Bearing CCR7 for Tumor Antigen Trafficking and Priming of T Cell Immunity in Melanoma. *Cancer Cell* (2016). doi:10.1016/j.ccell.2016.06.003
11. Salmon, H. *et al.* Expansion and Activation of CD103+Dendritic Cell Progenitors at the Tumor Site Enhances Tumor Responses to Therapeutic PD-L1 and BRAF Inhibition. *Immunity* (2016). doi:10.1016/j.immuni.2016.03.012
12. Ferris, S. T. *et al.* cDC1 prime and are licensed by CD4+ T cells to induce anti-tumour immunity. *Nature* (2020). doi:10.1038/s41586-020-2611-3
13. Binnewies, M. *et al.* Unleashing Type-2 Dendritic Cells to Drive Protective Antitumor CD4+ T Cell Immunity. *Cell* (2019). doi:10.1016/j.cell.2019.02.005
14. Broz, M. L. *et al.* Dissecting the Tumor Myeloid Compartment Reveals Rare Activating Antigen-Presenting Cells Critical for T Cell Immunity. *Cancer Cell* (2014). doi:10.1016/j.ccell.2014.09.007
15. Sánchez-Paulete, A. R. *et al.* Cancer immunotherapy with immunomodulatory anti-CD137 and anti–PD-1 monoclonal antibodies requires BATF3-dependent dendritic cells. *Cancer Discov.* (2016). doi:10.1158/2159-8290.CD-15-0510
16. Spranger, S., Bao, R. & Gajewski, T. F. Melanoma-intrinsic β-catenin signalling prevents anti-tumour immunity. *Nature* (2015). doi:10.1038/nature14404
17. Spranger, S., Dai, D., Horton, B. & Gajewski, T. F. Tumor-Residing Batf3 Dendritic Cells Are Required for Effector T Cell Trafficking and Adoptive T Cell Therapy. *Cancer Cell* (2017). doi:10.1016/j.ccell.2017.04.003
18. Marangoni, F. *et al.* Expansion of tumor-associated Treg cells upon disruption of a CTLA-4-dependent feedback loop. *Cell* (2021). doi:10.1016/j.cell.2021.05.027
19. Garris, C. S. *et al.* Successful Anti-PD-1 Cancer Immunotherapy Requires T Cell-Dendritic Cell Crosstalk Involving the Cytokines IFN-γ and IL-12. *Immunity* 1148–1161 (2018). doi:10.1016/j.immuni.2018.09.024
20. Maier, B. *et al.* A conserved dendritic-cell regulatory program limits antitumour immunity. *Nature* (2020). doi:10.1038/s41586-020-2134-y

21. Villani, A. C. *et al.* Single-cell RNA-seq reveals new types of human blood dendritic cells, monocytes, and progenitors. *Science (80-.).* (2017). doi:10.1126/science.aah4573

22. Dutertre, C. A. *et al.* Single-Cell Analysis of Human Mononuclear Phagocytes Reveals Subset-Defining Markers and Identifies Circulating Inflammatory Dendritic Cells. *Immunity* (2019). doi:10.1016/j.immuni.2019.08.008

23. Ginhoux, F., Guilliams, M. & Merad, M. Expanding dendritic cell nomenclature in the single-cell era. *Nature Reviews Immunology* (2022). doi:10.1038/s41577-022-00675-7

24. Brown, C. C. *et al.* Transcriptional Basis of Mouse and Human Dendritic Cell Heterogeneity. *Cell* (2019). doi:10.1016/j.cell.2019.09.035

25. Gerhard, G. M., Bill, R., Messemaker, M., Klein, A. M. & Pittet, M. J. Tumor-infiltrating dendritic cell states are conserved across solid human cancers. *Journal of Experimental Medicine* (2021). doi:10.1084/JEM.20200264

26. Pasqual, G. *et al.* Monitoring T cell-dendritic cell interactions in vivo by intercellular enzymatic labelling. *Nature* (2018). doi:10.1038/nature25442

27. Fidler, I. J. Biological Behavior of Malignant Melanoma Cells Correlated to Their Survival in Vivo. *Cancer Res.* (1975).

28. Basso, K. *et al.* Tracking CD40 signaling during germinal center development. *Blood* (2004). doi:10.1182/blood-2003-12-4291

29. Ghosh, S. & Hayden, M. S. New regulators of NF-κB in inflammation. *Nature Reviews Immunology* (2008). doi:10.1038/nri2423

30. Lee, E. G. *et al.* Failure to regulate TNF-induced NF-κB and cell death responses in A20-deficient mice. *Science (80-.).* (2000). doi:10.1126/science.289.5488.2350

31. Rossjohn, J., Pellicci, D. G., Patel, O., Gapin, L. & Godfrey, D. I. Recognition of CD1d-restricted antigens by natural killer T cells. *Nature Reviews Immunology* (2012). doi:10.1038/nri3328

32. Zimmerman, A. W. *et al.* Long-term engagement of CD6 and ALCAM is essential for T-cell proliferation induced by dendritic cells. *Blood* (2006). doi:10.1182/blood-2005-09-3881

33. Bailey, C. C., Zhong, G., Huang, I. C. & Farzan, M. IFITM-family proteins: The cell's first line of antiviral defense. *Annu. Rev. Virol.* (2014). doi:10.1146/annurev-virology-031413-085537

34. Kumanogoh, A. *et al.* Nonredundant roles of Sema4A in the immune system: Defective T cell priming and Th1/Th2 regulation in Sema4A-deficient mice. *Immunity* (2005). doi:10.1016/j.immuni.2005.01.014

35. Groettrup, M., Kirk, C. J. & Basler, M. Proteasomes in immune cells: More than peptide producers? *Nature Reviews Immunology* (2010). doi:10.1038/nri2687

36. Everitt, A. R. *et al.* IFITM3 restricts the morbidity and mortality associated with influenza. *Nature* (2012). doi:10.1038/nature10921

37. Tran, Q. *et al.* TMEM39A and human diseases: A brief review. *Toxicological Research* (2017). doi:10.5487/TR.2017.33.3.205

38. Decout, A., Katz, J. D., Venkatraman, S. & Ablasser, A. The cGAS–STING pathway as a therapeutic target in inflammatory diseases. *Nature Reviews Immunology* (2021). doi:10.1038/s41577-021-00524-z

39. Zhao, X. *et al.* CCL9 Is Secreted by the Follicle-Associated Epithelium and Recruits Dome Region Peyer's Patch CD11b + Dendritic Cells . *J. Immunol.* (2004). doi:10.4049/jimmunol.172.11.7220-a

40. Semmling, V. *et al.* Alternative cross-priming through CCL17-CCR4-mediated attraction of CTLs toward NKT cell-licensed DCs. *Nat. Immunol.* (2010). doi:10.1038/ni.1848

41. Coelho, A. L. *et al.* The Chemokine CCL6 Promotes Innate Immunity via Immune Cell Activation and Recruitment. *J. Immunol.* (2007). doi:10.4049/jimmunol.179.8.5474

42. Geijtenbeek, T. B. H. & Gringhuis, S. I. C-type lectin receptors in the control of T helper cell differentiation. *Nature Reviews Immunology* (2016). doi:10.1038/nri.2016.55

43. Wynn, T. A. Type 2 cytokines: Mechanisms and therapeutic strategies. *Nature Reviews Immunology* (2015). doi:10.1038/nri3831

44. Gatto, D. *et al.* The chemotactic receptor EBI2 regulates the homeostasis, localization and immunological function of splenic dendritic cells. *Nat. Immunol.* (2013). doi:10.1038/ni.2555

45. Li, J., Lu, E., Yi, T. & Cyster, J. G. EBI2 augments Tfh cell fate by promoting interaction with IL-2-quenching dendritic cells. *Nature* (2016). doi:10.1038/nature17947

46. Yi, T. & Cyster, J. G. EBI2-mediated bridging channel positioning supports splenic dendritic cell homeostasis and particulate antigen capture. *Elife* (2013). doi:10.7554/eLife.00757

47. Jinushi, M. *et al.* MFG-E8-mediated uptake of apoptotic cells by APCs links the pro- and antiinflammatory activities of GM-CSF. *J. Clin. Invest.* (2007). doi:10.1172/JCI30966

48. Jeon, M. S. *et al.* Essential role of the E3 ubiquitin ligase Cbl-b in T cell anergy induction. *Immunity* (2004). doi:10.1016/j.immuni.2004.07.013

49. Liberzon, A. *et al.* The Molecular Signatures Database Hallmark Gene Set Collection. *Cell Syst.* (2015). doi:10.1016/j.cels.2015.12.004

50. Subramanian, A. *et al.* Gene set enrichment analysis: A knowledge-based approach for interpreting genome-wide expression profiles. *Proc. Natl. Acad. Sci. U. S. A.* (2005). doi:10.1073/pnas.0506580102

51. Zilionis, R. *et al.* Single-Cell Transcriptomics of Human and Mouse Lung Cancers Reveals Conserved Myeloid Populations across Individuals and Species. *Immunity* (2019). doi:10.1016/j.immuni.2019.03.009

52. Yoshida, H. & Hunter, C. A. The immunobiology of interleukin-27. *Annual Review of Immunology* (2015). doi:10.1146/annurev-immunol-032414-112134

53. Fabbi, M., Carbotti, G. & Ferrini, S. Dual Roles of IL-27 in Cancer Biology and Immunotherapy. *Mediators of Inflammation* (2017). doi:10.1155/2017/3958069

54. Chihara, N. *et al.* Induction and transcriptional regulation of the co-inhibitory gene module in T cells. *Nature* (2018). doi:10.1038/s41586-018-0206-z

55. Zhu, J. *et al.* IL-27 gene therapy induces depletion of Tregs and enhances the efficacy of cancer immunotherapy. *JCI insight* (2018). doi:10.1172/jci.insight.98745

56. Groom, J. R. *et al.* CXCR3 Chemokine Receptor-Ligand Interactions in the Lymph Node Optimize CD4+ T Helper 1 Cell Differentiation. *Immunity* (2012). doi:10.1016/j.immuni.2012.08.016

57. Mikucki, M. E. *et al.* Non-redundant requirement for CXCR3 signalling during tumoricidal T-cell trafficking across tumour vascular checkpoints. *Nat. Commun.* (2015). doi:10.1038/ncomms8458

58. Horton, B. L. *et al.* Lack of CD8+T cell effector differentiation during priming mediates checkpoint blockade resistance in non-small cell lung cancer. *Sci. Immunol.* (2021). doi:10.1126/sciimmunol.abi8800

59. Bauer, C. A. *et al.* Dynamic Treg interactions with intratumoral APCs promote local CTL dysfunction. *J. Clin. Invest.* (2014). doi:10.1172/JCI66375

60. Vinay, D. S. *et al.* Immune evasion in cancer: Mechanistic basis and therapeutic strategies. *Seminars in Cancer Biology* (2015). doi:10.1016/j.semcancer.2015.03.004

61. Cubillos-Ruiz, J. R. *et al.* ER Stress Sensor XBP1 Controls Anti-tumor Immunity by Disrupting Dendritic Cell Homeostasis. *Cell* (2015). doi:10.1016/j.cell.2015.05.025

62. Scarlett, U. K. *et al.* Ovarian cancer progression is controlled by phenotypic changes in dendritic cells. *J. Exp. Med.* (2012). doi:10.1084/jem.20111413

63. Corbett, T. H., Griswold, D. P., Roberts, B. J., Peckham, J. C. & Schabel, F. M. Tumor Induction Relationships in Development of Transplantable Cancers of the Colon in Mice for Chemotherapy Assays, with a Note on Carcinogen Structure. *Cancer Res.* (1975).

64. Marson, A. *et al.* Foxp3 occupancy and regulation of key target genes during T-cell stimulation. *Nature* (2007). doi:10.1038/nature05478

65. Rotman, J., Koster, B. D., Jordanova, E. S., Heeren, A. M. & de Gruijl, T. D. Unlocking the therapeutic potential of primary tumor-draining lymph nodes. *Cancer Immunology, Immunotherapy* (2019). doi:10.1007/s00262-019-02330-y

66. Kitano, M. *et al.* Imaging of the cross-presenting dendritic cell subsets in the skin-draining lymph node. *Proc. Natl. Acad. Sci. U. S. A.* (2016). doi:10.1073/pnas.1513607113

67. Nowotschin, S. & Hadjantonakis, A. K. Use of KikGR a photoconvertible green-to-red fluorescent protein for cell labeling and lineage analysis in ES cells and mouse embryos. *BMC Dev. Biol.* (2009). doi:10.1186/1471-213X-9-49

68. Tsutsui, H., Karasawa, S., Shimizu, H., Nukina, N. & Miyawaki, A. Semi-rational engineering of a coral fluorescent protein into an efficient highlighter. *EMBO Rep.* (2005). doi:10.1038/sj.embor.7400361

69. Chen, B., Zhu, L., Yang, S. & Su, W. Unraveling the Heterogeneity and Ontogeny of Dendritic Cells Using Single-Cell RNA Sequencing. *Frontiers in Immunology* (2021). doi:10.3389/fimmu.2021.711329

70. Esterházy, D. *et al.* Classical dendritic cells are required for dietary antigen-mediated induction of peripheral T reg cells and tolerance. *Nat. Immunol.* (2016). doi:10.1038/ni.3408

71. Esterházy, D. *et al.* Compartmentalized gut lymph node drainage dictates adaptive immune responses. *Nature* (2019). doi:10.1038/s41586-019-1125-3

72. Giladi, A. *et al.* Dissecting cellular crosstalk by sequencing physically interacting cells. *Nat. Biotechnol.* (2020). doi:10.1038/s41587-020-0442-2

73. Altman, J. D. *et al.* Phenotypic analysis of antigen-specific T lymphocytes. *Science (80-.).* (1996). doi:10.1126/science.274.5284.94

74. Krishnamurty, A. T. *et al.* Somatically Hypermutated Plasmodium-Specific IgM+ Memory B Cells Are Rapid, Plastic, Early Responders upon Malaria Rechallenge. *Immunity* (2016). doi:10.1016/j.immuni.2016.06.014

75. Cohen, M. *et al.* The interaction of CD4+ helper T cells with dendritic cells shapes the tumor microenvironment and immune checkpoint blockade response. *Nat. Cancer* (2022). doi:10.1038/s43018-022-00338-5

76. Lesley, R., Kelly, L. M., Xu, Y. & Cyster, J. G. Naive CD4 T cells constitutively express CD40L and augment autoreactive B cell survival. *Proc. Natl. Acad. Sci. U. S. A.* (2006). doi:10.1073/pnas.0601539103

77. Grewal, I. S. & Flavell, R. A. The Role of CD40 Ligand in Costimulation and T-Cell Activation. *Immunol. Rev.* (1996). doi:10.1111/j.1600-065x.1996.tb00921.x

78. Döhler, A. *et al.* RelB+ steady-state migratory dendritic cells control the peripheral pool of the natural Foxp3+ regulatory T cells. *Front. Immunol.* (2017). doi:10.3389/fimmu.2017.00726

79. Borst, J., Ahrends, T., Bąbała, N., Melief, C. J. M. & Kastenmüller, W. CD4+ T cell help in cancer immunology and immunotherapy. *Nature Reviews Immunology* (2018). doi:10.1038/s41577-018-0044-0

80. Bennett, S. R. M. *et al.* Help for cytotoxic-T-cell responses is mediated by CD4O signalling. *Nature* (1998). doi:10.1038/30996

81. Schoenberger, S. P., Toes, R. E. M., Van Dervoort, E. I. H., Offringa, R. & Melief, C. J. M. T-cell help for cytotoxic T lymphocytes is mediated by CD40-CD4OL interactions. *Nature* (1998). doi:10.1038/31002

82. Ridge, J. P., Di Rosa, F. & Matzinger, P. A conditioned dendritic cell can be a temporal bridge between a CD4 + T-helper and a T-killer cell. *Nature* (1998). doi:10.1038/30989

83. Banchereau, J. & Steinman, R. M. Dendritic cells and the control of immunity. *Nature* (1998). doi:10.1038/32588

84. Mellman, I. & Steinman, R. M. Dendritic cells: Specialized and regulated antigen processing machines. *Cell*

(2001). doi:10.1016/S0092-8674(01)00449-4

85. Oliveira, M. M. S. & Westerberg, L. S. Cytoskeletal regulation of dendritic cells: An intricate balance between migration and presentation for tumor therapy. *Journal of Leukocyte Biology* **108**, 1051–1065 (2020).

86. Castellino, F. *et al.* Chemokines enhance immunity by guiding naive CD8+T cells to sites of CD4+T cell-dendritic cell interaction. *Nature* (2006). doi:10.1038/nature04651

87. Murugaiyan, G. & Saha, B. IL-27 in tumor immunity and immunotherapy. *Trends in Molecular Medicine* (2013). doi:10.1016/j.molmed.2012.12.002

88. Hu, A. *et al.* Intra-Tumoral Delivery of IL-27 Using Adeno-Associated Virus Stimulates Anti-tumor Immunity and Enhances the Efficacy of Immunotherapy. *Front. Cell Dev. Biol.* (2020). doi:10.3389/fcell.2020.00210

89. Kilgore, A. M. *et al.* IL-27p28 Production by XCR1 + Dendritic Cells and Monocytes Effectively Predicts Adjuvant-Elicited CD8 + T Cell Responses . *ImmunoHorizons* (2018). doi:10.4049/immunohorizons.1700054

90. Pennock, N. D., Gapin, L. & Kedl, R. M. IL-27 is required for shaping the magnitude, affinity distribution, and memory of T cells responding to subunit immunization. *Proc. Natl. Acad. Sci. U. S. A.* (2014). doi:10.1073/pnas.1407393111

91. Wei, J. *et al.* Critical Role of Dendritic Cell–Derived IL-27 in Antitumor Immunity through Regulating the Recruitment and Activation of NK and NKT Cells. *J. Immunol.* (2013). doi:10.4049/jimmunol.1300328

92. Woo, S. R. *et al.* STING-dependent cytosolic DNA sensing mediates innate immune recognition of immunogenic tumors. *Immunity* (2014). doi:10.1016/j.immuni.2014.10.017

93. Madsen, L. *et al.* Mice lacking all conventional MHC class II genes. *Proc. Natl. Acad. Sci. U. S. A.* (1999). doi:10.1073/pnas.96.18.10338

94. Lee, P. P. *et al.* A critical role for Dnmt1 and DNA methylation in T cell development, function, and survival. *Immunity* (2001). doi:10.1016/S1074-7613(01)00227-8

95. Hogquist, K. A. *et al.* T cell receptor antagonist peptides induce positive selection. *Cell* (1994). doi:10.1016/0092-8674(94)90169-4

96. Barnden, M. J., Allison, J., Heath, W. R. & Carbone, F. R. Defective TCR expression in transgenic mice constructed using cDNA- based α- and β-chain genes under the control of heterologous regulatory elements. *Immunol. Cell Biol.* (1998). doi:10.1046/j.1440-1711.1998.00709.x

97. Caton, M. L., Smith-Raska, M. R. & Reizis, B. Notch-RBP-J signaling controls the homeostasis of CD8-dendritic cells in the spleen. *J. Exp. Med.* (2007). doi:10.1084/jem.20062648

98. Quadros, R. M. *et al.* Easi-CRISPR: A robust method for one-step generation of mice carrying conditional and insertion alleles using long ssDNA donors and CRISPR ribonucleoproteins. *Genome Biol.* (2017). doi:10.1186/s13059-017-1220-4

99. Engels, B. *et al.* Retroviral vectors for high-level transgene expression in T lymphocytes. *Hum. Gene Ther.* (2003). doi:10.1089/104303403322167993

100. Szymczak, A. L. & Vignali, D. A. A. Development of 2A peptide-based strategies in the design of multicistronic vectors. *Expert Opinion on Biological Therapy* (2005). doi:10.1517/14712598.5.5.627

101. Trombetta, J. J. *et al.* Preparation of single-cell RNA-Seq libraries for next generation sequencing. *Curr. Protoc. Mol. Biol.* (2014). doi:10.1002/0471142727.mb0422s107

102. Hao, Y. *et al.* Integrated analysis of multimodal single-cell data. *Cell* (2021). doi:10.1016/j.cell.2021.04.048

103. Korotkevich, G., Sukhov, V. & Sergushichev, A. Fast gene set enrichment analysis. bioRxiv. (2019).

104. Love, M. I., Huber, W. & Anders, S. Moderated estimation of fold change and dispersion for RNA-seq data with DESeq2. *Genome Biol.* (2014). doi:10.1186/s13059-014-0550-8

105. Stephens, M. False discovery rates: A new deal. *Biostatistics* (2017). doi:10.1093/biostatistics/kxw041